ROYAL INSTITUTE
OF TECHNOLOGY

Surface Reactivity and Electronic Structure of Metal Oxides

ANNELI ÖNSTEN

Doctoral Thesis
Stockholm, Sweden 2011

KTH, Royal Institute of Technology
School of Information and
Communication Technology
Materials Physics
SE-164 40 Stockholm
SWEDEN

TRITA-ICT/MAP AVH Report 2011:07
ISSN 1653-7610
ISRN KTH/ICT-MAP/AVH-2011:07-SE
ISBN 978-91-7415-995-0

Akademisk avhandling som med tillstånd av Kungl Tekniska högskolan framlägges till offentlig granskning för avläggande av teknologie doktorsexamen i Mikroelektronik och tillämpad fysik måndagen den 30 maj 2011, klockan 10.00 i Sal C2, KTH-Electrum, Isafjordsgatan 26, Kista, Stockholm.

Tryck: Kista Snabbtryck AB

Abstract

The foci of this thesis are the metal oxides Cu_2O, ZnO and Fe_3O_4 and their interaction with water and sulfur dioxide (SO_2). The intention is to study SO_2-induced atmospheric corrosion on a molecular level. All studies are based on photoelectron spectroscopy (PES) and scanning tunneling microscopy (STM) measurements.

The band structure of Cu_2O in the Γ-M direction has been probed by angle-resolved PES (ARPES). It reveals a more detailed picture of the bulk band structure than earlier data and gives the first experimental evidence of a dispersive hybridized Cu $3d$-Cu $4s$ state. The experimental data is compared to band structure calculations.

The structure of clean metal oxide surfaces and impact of sample preparation have been studied. Oxygen vacancies can form a $(\sqrt{3}\times\sqrt{3})$R30° reconstruction on $Cu_2O(111)$. Oxygen atoms adjacent to copper vacancies, steps or kinks are shown to be adsorption sites for both water and SO_2. Annealing temperature influences the defect density and hydrogen content in ZnO, which can have large impact on the surface properties of ZnO(0001).

Water is shown to adsorb dissociatively on ZnO(0001) and partly dissociatively on $Cu_2O(111)$. The dissociation occurs at undercoordinated oxygen sites on both surfaces. Water stays adsorbed on ZnO(0001) at room temperature but on $Cu_2O(111)$, all water has desorbed at 210 K.

SO_2 interacts with one or two undercoordinated O-sites on all studied oxide surfaces forming SO_3 or SO_4 species respectively. SO_4 on $Fe_3O_4(100)$ follows the $(\sqrt{2}\times\sqrt{2})$R45° reconstruction. On $Cu_2O(111)$ and ZnO(0001), SO_2 adsorbs on defect sites. An SO_3 to SO_4 transition is observed on $Cu_2O(111)$ when heating an SO_3 adsorbate layer from 150 K to 280 K.

Coadsorption of water and SO_2 on ZnO(0001) and $Fe_3O_4(100)$ has been studied briefly. Water blocks SO_2 adsorption sites on ZnO(0001). On $Fe_3O_4(100)$ and on one type of reduced ZnO(0001) sample, SO_2 dissociation to atomic sulfur or sulfide occurs to a higher extent on water exposed surfaces than on clean surfaces. Water thus appears to increase the charge density on some surfaces. Further studies are needed to reveal the cause of this unexpected effect.

Keywords: oxides, surfaces, defects, cuprous oxide, zinc oxide, magnetite, water, OH, sulfur dioxide, photoelectron spectroscopy, scanning tunneling microscopy

Acknowledgements

I get by with a little help from my friends.

The Beatles (Sgt. Pepper's Lonely Hearts Club Band, 1967)

First, I would like to thank my primary supervisor Prof. Ulf Karlsson for helping me with important matters and for inspiring me along the way. Thanks also for being supportive, for interesting and enjoyable conversations at coffee and lunch breaks and to you and your wife Hua for being great travel companions in China.

I am also very grateful to my supervisor, Doc. Mats Göthelid for learning me most of what I know about surface science, for motivating me and for guiding and helping me all the way to the end. Thank you also for making work much more fun by singing opera in the lab, whistling in the corridor and for your good sense of humor. It has been a pleasure to work with you.

I am glad to have experienced a close and fruitful collaboration with Dr. Dunja Stoltz, whose frank and friendly attitude I have appreciated. Thank you for being considerate and such a good colleague and friend.

Many thanks to Dr. Jonas Weissenrieder. Your extensive experience in my field of study has been invaluable and inspiring for me. I am also grateful for your friendly and helpful attitude, which enables me to ask you so many questions and I enjoyed working with you.

Another person that I am indebted to is Dr. Pål Palmgren, for a lot of help with experimental trials and useful discussions. Without the use of your technical skills, e.g. for fixing old broken equipment, I would have been totally lost in the lab when I started as a PhD student. Thanks also for the fun we had in the good old time when we shared office.

Then I would like to thank all the present and former Surface Physics group members. I am grateful for all discussions with Dr. Marcelo Zuleta about science and about life in general, which meant a lot to me. Moreover your expertise in chemistry has been valuable for me. Thanks also to Dr. Karolina for all the walking and talking and for the many laughs together. Shun Yu the brave is thanked for all the great help in the labs, for having been a splendid guide in China and an excellent officemate. I am also grateful to Sareh Ahmadi for your help in the lab, for being thoughtful and supportive and good to talk to. Moreover, I would like to thank Dr. Winnie Chow for your positive attitude well contributing to the positive atmosphere in our group. Your, Sarehs and Shuns persistent fight with the new whilful STM impressed me. I also very much enjoyed the time with my former colleagues Dr. Diana Orrling and Dr. Björn Agnarsson, who together with Pål and

Mats introduced me to the lab. Pooya Tabib Zadeh Adibi is gratefully acknowledged for being friendly and easy to work with. Thanks also to the master thesis workers Zarah Besharat for always being so considerate and friendly and to Athanasios Revenikiotis, since your positive attitude and professional tip production made life in the lab much nicer. My gratitude to Dr. Peter Niraj Nirmalraj and Dr. Priya Chakrapani for their kindness and I really appreciated you inviting me to the feast at the Hindu temple. I would also like to thank Dr. Ikenna Nlebedim for giving interesting discussions at the lunch table. Moreover I would like to thank Dr. Mats Leandersson for help in the lab and thanks to Marianne, Christofer, Marcus, Milan and all other people that have been working in our group.

Dr. Martin Månsson, Dr. Thomas Claesson and Prof. Oscar Tjernberg are gratefully acknowledged for convincing me to join you to the unforgettable trip to Spring-8 in Japan. It was very fun working with you and it also gave me a push in the right direction in my PhD work. I would also like to thank you for the extensive and invaluable help with finishing the final version of the manuscript about the valence band structure of Cu_2O, which is by far my most cited article and gives me a warm feeling every time I look at it.

Many thanks to the current department administrator Madeleine Printzsköld for being so helpful, thoughtful and professional. You are a fresh breath of air at the department and I could not emphasize enough how much the installing of the new coffee machine helped me in finishing my thesis.

Thanks a lot to the former department administrator Marianne Widing, who has been excellent and helpful in her work. Thank you also for always having been so considerate, supportive, observant of every persons well-being and involved in every persons life in the department.

My gratitude to Prof. Birger Emmoth who passed away in 2009, which was a great loss for the department. He was a very kind person, who shared interesting stories from his life and he was always helpful.

I would like to thank all the people at the department of Materials Physics at KTH: Thanks to Ben for being an excellent officemate and such a nice guy, to Dr. Stefano and Yeyu for letting me disturb you so many times and for interesting discussions about everything and nothing, to Magnus, Olof and Prof. Oscar for the many fun and inspiring lunch breaks together. Thanks to Prof. Jan Linnros who often was the only corridor-company late friday evenings, Mahtab and all other friendly people in the group of Prof. Jan and in the spin-group led by Prof. Johan Åkerman. You were all the reason why I went most of the days to work with a positive feeling. I will miss all of you a lot.

Andreas, alias the computer-guy is acknowledged for all computer-related help and the people in the ELAB Electrumlab are thanked for their help with providing equipment. Vytautas is thanked for making lunch breaks more fun and for finding words when I and others couldn't. I also want to thank Anna Sahlholm for always being friendly and good to talk to.

Dr. Franz Hennies, Dr. Annette Pietzsch, the former beam-line managers at I511, Dr. Stefan Wiklund and all other helpful staff at MAX-lab are gratefully

acknowledged for all the help and support during beamtimes.

Thanks to Prof. Christofer Leygraf, Dr. Jonas Hedberg, Doc. Laurent Duda, Prof. Joseph Nordgren, Dr. Johan Persson and Dr. Teodor Aastrup for the collaboration and interesting discussions.

Prof. Dinko Chakarov, Dr. Hans Persson and Dr. Lars Ilver are thanked for helping me when working in their lab at Chalmers. Special thanks to Dr. Lars Ilver for your invaluable experimental help. Your skills e.g. with fixing old broken electronic equipment really impressed me.

Another person that has been important for me is Prof. Arne Rosén, who recommended me for this PhD position and who increased my interest in spectroscopy in his course, Atomic and molecular spectroscopy, at Chalmers. Thank you!

A sincere gratitude to the beautiful $Cu_2O(111)$ crystal. Even though I caused your fracture into several pieces, you delivered many satisfying results.

Finally I would like to thank my lovely family: Henrik whose help and patience has been invaluable for finishing my thesis and 'min lilla solstråle' Leo (Leonard), you are the loves of my life. Many thanks to my relatives and almost relatives: mamma, Sören, Per, pappa, Elisabeth, Emelie, Gunilla, Björn, Ulf, Kristina, Pia, Chris, Henriks great grandmother Margot, Tina, Janne, Simon, Alice, Karin, Anders and other relatives. You mean a lot to me. Special thanks to pappa, Elisabeth, Pia and Chris who helped with babysitting in the end of writing my thesis. I also would like to thank my friends: Sara, Therese, Haninge-gänget, Marika and other friends. From now on I want to spare more time to see you!

Andreas Lundgren is especially acknowledged for reading through and correcting one of my manuscripts.

My cousin Karin deserves special thanks for letting me live in her apartment for at least one month in Gothenburg when I worked in a lab at Chalmers and for giving me company (by phone) and keeping me awake during some of the nightshifts at MAX-lab. Skriv snart snälla söta. Annars anfaller avsändaren.

Last but not least I would like to mention my grandparents and especially my grandmother Maj-Britt (1922-2004) with whom I spent much time as a child. She has meant a lot to me and has been a source of inspiration in my life.

Without the help from these people (and especially one crystal), this thesis would not have been possible.

Publications

List of papers included in this thesis:

1. A. Önsten, M. Månsson, T. Claesson, T. Muro, T. Matsushita, T. Nakamura, T. Kinoshita, U. O. Karlsson, and O. Tjernberg, Probing the valence band structure of Cu_2O using high-energy angle-resolved photoelectron spectroscopy, *Phys. Rev. B*, 76:115127, 2007.

2. A. Önsten, M. Göthelid, and U. O. Karlsson, Atomic structure of $Cu_2O(111)$, *Surf. Sci.*, 603:257, 2009.

3. A. Önsten, J. Weissenrieder, D. Stoltz, S. Yu, M. Göthelid, and U. O. Karlsson, Role of defects in surface chemistry on $Cu_2O(111)$, *manuscript*, 2011.

4. A. Önsten, D. Stoltz, P. Palmgren, S. Yu, M. Göthelid, and U. O. Karlsson, Water Adsorption on ZnO(0001): Transition from Triangular Surface Structures to a Disordered Hydroxyl Terminated phase, *J. Phys. Chem. C*, 114:11157, 2010.

5. A. Önsten, D. Stoltz, P. Palmgren, S. Yu, T. Claesson, M. Göthelid, and U. O. Karlsson, SO_2 Interaction with Zn(0001) and ZnO(0001) and the Influence of Water, *manuscript*, 2011.

6. D. Stoltz, A. Önsten, U. O. Karlsson, and M. Göthelid, High resolution spectroscopic and microscopic signatures of ordered growth of ferrous sulfate in SO_2 assisted corrosion of $Fe_3O_4(100)$, *Appl. Phys. Lett.*, 91:093107, 2007.

List of papers not included in this thesis:

1. D. Stoltz, A. Önsten, U. O. Karlsson, and M. Göthelid, Scanning Tunneling Microscopy of Fe- and O-sublattices on $Fe_3O_4(100)$, *Ultramicroscopy*, 108:540, 2008.

2. D. Stoltz, A. Önsten, J. Weissenrieder, U. O. Karlsson, and M. Göthelid, Dry oxidation of SO_2 to SO_4 on $(\sqrt{2} \times \sqrt{2})$R45° $Fe_3O_4(100)$ observed by STM, *manuscript*, 2011.

3. P. Palmgren, T. Claesson, A. Önsten, B. Agnarsson, M. Månsson, O. Tjernberg, and M. Göthelid, Band bending and structure dependent HOMO at the ZnO(0001)-TiOPc interface, *Surf Sci.*, 601:4222, 2007.

4. T. Claesson, M. Månsson, A. Önsten, M. Shi, Y. Sassa, S. Pailhes, J. Chang, A. Bendounan, L. Patthey, J. Mesot, T. Muro, T. Matsushita, T. Kinoshita, T. Nakamura, N. Momono, M. Oda, M. Ido, and O. Tjernberg, Electronic structure of $La_{1.48}Nd_{0.4}Sr_{0.12}CuO_4$ probed by high- and low-energy angle-resolved photoelectron spectroscopy, *Phys. Rev. B*, 80:094503, 2009.

5. B. Brena, P. Palmgren, K. Nilson, Shun Yu, F. Hennies, B. Agnarsson, A. Önsten, M. Månsson, and M. Göthelid, InSb-TiOPc interfaces: band alignment, ordering and structure dependent HOMO splitting, *Surf. Sci.*, 603:3160, 2009.

Abbreviations

ARPES	**A**ngle-**r**esolved **p**hoto**e**lectron **s**pectroscopy
CSA	**C**oordinatively **sa**turated
CUS	**C**oordinatively **uns**aturated
DFT	**D**ensity **f**unctional **t**heory
HOMO	**H**ighest **o**ccupied **m**olecular **o**rbital
L	**L**angmuir (1 L = 10^{-6} torr s)
LDA	**L**ocal **d**ensity **a**pproximation
LEED	**L**ow **e**nergy **e**lectron **d**iffraction
LUMO	**L**owest **u**noccupied **m**olecular **o**rbital
MCUS	**M**ultiply **c**oordinatively **uns**aturated
PES	**P**hoto**e**lectron **s**pectroscopy
STM	**S**canning **t**unneling **m**icroscopy
STS	**S**canning **t**unneling **s**pectroscopy
UHV	**U**ltra**h**igh **v**acuum

Contents

Chapter 1

Introduction

The beginning of knowledge is the discovery of something we do not understand.

Frank Herbert (1920 - 1986)

Surface chemistry on metal oxides plays an important role in modern society. Metal oxides are widely used catalyst materials. Catalysts are of paramount importance in the chemical industry and they will play a key role in solving many of the challenging problems that the future holds, e.g. in the energy sector when oil resources start to run short. Moreover, interaction between metal oxides and the ambient atmosphere is highly important in the corrosion of metals, which is a major cost for society. The initial motivation for the work behind this thesis was to study atmospheric corrosion and therefore, a short introduction to this field is appropriate.

Atmospheric corrosion is the most commonly occurring corrosion process of metals and it has been described in detail by Leygraf and Graedel [1]. It is a rather complex phenomenon, since it involves three phases, i.e. a solid, a liquid and a gaseous phase. The solid phase is generally considered as a metal surface with a layer of oxide or hydroxide, the liquid is an aqueous layer and the gas is the atmosphere. In a simplified picture, atmospheric corrosion can be divided into three types of stages, i.e. the initial stages that occur in a fraction of a second, the intermediate stages and the final stages that occur after several years or even decades.

In the *intial stages*, water adsorbs on the surface. The first layer of water can adsorb both as molecules or dissociate forming hydroxyl groups on the oxide surface. For most engineering applications, polycrystalline materials are used and on these types of surfaces, the first layer water normally consists of hydroxyl groups. The second and subsequent monolayers of water consist of molecular water and the thickness of the aqueous layer depends on humidity. At a relative humidity exceeding 40% and at room temperature the water layer is 2-10 monolayers thick, or on certain surfaces even thicker [1].

In the *intermediate stages*, gases or particles in the atmosphere, e.g. the gas SO_2 dissolves into the aqueous layer. This is followed by reactions in the liquid layer, e.g. formation of bisulfite ions (HSO_3^-), bisulfate ions (HSO_4^-) and protons. The next step is called *proton- and ligand-induced metal dissolution*. This step has

been recognized as one of the most important processes in the intermediate stages of atmospheric corrosion, although it is not fully understood at a molecular level [1]. The process involves exchange of hydroxyl ions at the metal oxide surface with ions in the water layer such as protons, bisulfite and bisulfate ions. Bond weakening and metal dissolution have been shown to be the result of such mechanisms. The dissolved metal ions, e.g. Fe^{2+}, can then bind to counterions, e.g. SO_3^{2-} in the water layer and this is called *ion pairing*. When the concentration of the ion pairs reach saturation, they precipitate into a solid phase. Surface defects can often serve as nucleation sites for precipitation.

In the *final stages* of atmospheric corrosion, the corrosion products coalesce until they completely covers the surface. The proceeding growth of the layer of corrosion products is very dependent upon exposure conditions, i.e. if it takes place indoors or outdoors, in humid or damp conditions, in rural or urban areas etc.

The work presented in this thesis is part of a frame program, whose focus is to study the interfacial regime between a solid and an atmosphere. This project is a collaboration involving three other research groups, i.e. Department of Materials Science and Engineering at KTH, Department of Physics at Uppsala University and Attana AB, Stockholm. There were three main aims for this project and two of them involved the Materialfysik group. These aims were:

- to obtain a molecular understanding of formation and properties of the aqueous adlayer on single- and polycrystalline metal oxide model surfaces;
- to extend our molecular understanding of the role of SO_2 on initial atmospheric corrosion on model oxides with high SO_2 reactivity (e.g. MgO), intermediate (e.g. copper, nickel and zinc oxides) and low SO_2-reactivity (iron oxides).

The task of the Materialfysik group was to use scanning tunneling microscopy (STM) and high-resolution photoelectron spectroscopy (PES) to study water and SO_2 adsorption and coadsorption on single crystalline metal oxide surfaces.

In order to reach a good level of understanding of the SO_2 induced corrosion on different metals at a fundamental level, using surface scientific methods, one approach would be as follows. First, a few key metals, e.g. magnesium, iron and copper should be chosen. Then some of the most commonly occurring oxides or corrosion products for these metals should be identified, e.g. Fe_3O_4, FeOOH [1] and iron sulfates for iron. In addition, the most frequently occurring surfaces of these compounds, such as (111), (110) and (100) for materials with cubic structures should be identified. Then if we have three types of metals, three corrosion products for each metal and three surfaces for each corrosion product, we end up with 27

[1] It should be noted that many of the corrosion products formed on metal surfaces can be hard to obtain or produce in single crystalline form. Furthermore, if it is possible to obtain a single crystalline sample of e.g. FeOOH, it might be very hard to prepare a clean and well-ordered surface from this sample

different samples. Some of these samples will be hard to prepare to obtain clean and well-ordered surfaces and for many oxide surfaces, the exact atomic structure is not known. A lot of work is thus needed to understand the structure and properties of the clean surfaces. Moreover, different surface preparations can give rise to different surface terminations, which might need some attention. Then, after all this work, we arrive at the initial aim of this study, to study adsorption and coadsorption of water and sulfur dioxide on these surfaces. Moreover, in order for these studies to be comparable to atmospheric conditions, UHV studies must be complemented with measurements at higher pressures. Every surface scientist knows how time demanding studies of only one sample surface can be and will soon realise that the type of project described above is a mission impossible, at least in the situation normally found on a research department, where one or a few people are working on the same subject.

Coming back to the work presented here, our group ended up with studying water and SO_2 adsorption on the three surfaces $Cu_2O(111)$, ZnO(0001) and $Fe_3O_4(100)$. The motivation for choosing these surfaces was partly their relevance in surface chemical processes, their abundance in nature and their interesting properties. However, the choice of materials and surfaces was also based on the group's knowledge on how to prepare and clean these sample surfaces, since this can be a time-consuming process. In order to get a clear picture of the adsorption mechanisms on a surface, the atomic structure of the surface has to be known. For all the studied surfaces, it was discovered that the atomic structure was not fully known or that different surface properties could be obtained with different cleaning procedures. Therefore the clean bulk and surface properties deserved to be studied and results and discussion from these studies can be found in chapter 3. In chapter 4, the water and SO_2 adsorption studies on the different surfaces are presented side by side in order to compare the different systems.

The research findings in this thesis might appear as 'a drop in the ocean', when trying to understand the SO_2-induced atmospheric corrosion process. Still, it is important to see that these types of studies are required to understand chemical and physical surface properties at a fundamental level and this is of course the ultimate goal of fundamental research. One has to be aware of that the process to reach a good level of knowledge on an oxide surface and its interaction with molecules can be long and tedious. However, when reaching that point, the knowledge acquired can be used not only to understand corrosion processes but for a wide range of phenomena such as catalysis, gas sensors, emission control and perhaps for applications not yet discovered.

Chapter 2

Experimental methods

The experimental data presented in this thesis is acquired with several different techniques. The techniques complement each other by answering different questions. Scanning tunneling microscopy (STM) gives for example local information about the atomic structure while the structural information obtained with low-energy electron diffraction (LEED) is averaged over a larger surface area. On the other hand, STM images from a few spots on a surface might not well represent the whole surface. It is also important to examine whether one can come to the same conclusion from the results from two or more techniques, since this will increase the reliability of the conclusion. A combination of STM and photoelectron spectroscopy (PES) can be very valuable, e.g. when identifying different surface sites.

In order to investigate surface properties at the atomic/molecular level, the surfaces under study must be well-defined and clean. This is why the majority of surface science studies including the studies presented in this thesis, are performed at ultrahigh vacuum (UHV) conditions. Working at UHV conditions can be quite cumbersome and time consuming and there is a whole science devoted to it. Therefore, this chapter starts with a section about vacuum technology. Furthermore, a section is dedicated to sample preparation, since this is an important part of surface science experiments. This is followed by a short introduction to the experimental techniques used for obtaining the data introduced in this thesis.

2.1 Vacuum technology

The meaning of the word vacuum is absence of molecules/atoms. However, the complete absence of all molecules do not exist anywhere, there are just degrees of vacuum. Vacuum can be classified into three pressure (p) ranges: rough (low) vacuum (p$\approx$1000-10^{-3} mbar), high vacuum (p$\approx$$10^{-3}$-$10^{-8}$ mbar) and ultrahigh vacuum (UHV, p$\lesssim$$10^{-8}$ mbar) [2]. At p$\gtrsim$ 10^{-2} mbar, the gaseous flow is *viscous* meaning that it behaves similar to a liquid when it moves and has internal friction

[2]. At lower pressures, the molecules move in an arbitrary fashion and then we have *molecular* flow.

The base pressure in vacuum chambers used in surface science experiments is typically around $1{\cdot}10^{-10}$ mbar. There are mainly two reasons that such a good vacuum is needed; first to obtain a clean and well-defined surface and second, to enable the use of experimental techniques where low-energy electrons and ions are used.

In order to obtain a pressure of $\sim 1{\cdot}10^{-10}$ mbar, a combination of pumps is needed, since different types of pumps can be used only in certain pressure ranges. Pumps that are used to obtain UHV conditions such as ion pumps and cryo pumps need a maximum pressure of 10^{-3}-10^{-6} mbar to be able to start. Therefore, normally turbo pumps are combined with ion or cryo pumps. Moreover, most turbo pumps require a starting pressure of 10^{-2}-10^{-3} mbar and are therfore 'backed' with pumps such as the rotary pump. When the inside of a UHV chamber is exposed to air, all surfaces will be covered with a layer of water. Since water has a high vapor pressure, pumping on the water layer will result in a slow desorption and it will take a very long time to reach UHV conditions. Therefore, UHV chambers are 'baked', i.e. they are heated to $\sim 150^{\circ}$C to speed up the degassing process. This bake-out process takes from 12h to a few days. Moreover, degassing properties are important to consider when chosing materials to use in the vacuum chambers. Materials such as zinc with high vapor pressure are not suitable in vacuum chambers, especially not for parts that are to be heated. Suitable materials for the UHV chamber are e.g. stainless steel, aluminum, titanium and copper. Depending on application, many different types of materials are used in a vacuum chamber.

2.2 Sample preparation

Most materials used in real-world, every-day applications are polycrystalline or amorphous, giving a large number of exposed crystallographic planes and an even higher number of exposed surface sites. In order to understand in detail the interaction between atoms or molecules and a solid surface, one has to know the exact surface sites where the reaction takes place. Therefore, in surface science experiments, single crystalline surfaces are preferred since they are well-defined and have a relatively small number of surface sites. However, it is not always straight forward to obtain clean, regular and well-defined single crystalline surfaces and there are several methods that can be used, e.g. cleavage in vacuum, sputtering and annealing cycles, evaporation, molecular beam epitaxy and chemical beam epitaxy [3].

In the work presented here, all sample surfaces have been prepared by means of sputtering and annealing. Sputtering involves bombarding the sample with noble gas ions. First the UHV chamber is filled with clean noble gas such as Argon to a certain pressure (often 10^{-5}- 10^{-3} mbar). Then the sample is exposed to a beam of noble gas ions that are created in a sputter gun. In the sputter gun, a

high current is run through a filament, leading to a high temperature and emission of electrons. A voltage in the sputter gun accelerates the electrons through the noble gas, which produces ions. The ion beam is focused on the sample by a high voltage, typically 0.5-3 kV. Ions that bombard the sample surface will remove the outermost atomic layers and leave a rough and disordered surface. Therefore, a subsequent annealing is performed to obtain a more smooth and well-ordered sample surface. Unfortunately, annealing can sometimes also result in the diffusion of impurity atoms in the bulk to the surface. The heating can be made resistively or by bombarding electrons on the backside of the sample. The sputtering-annealing cycle is then repeated until a good low-energy electron diffraction (LEED) pattern is obtained and no impurities are found by auger electron spectroscopy (AES) or x-ray photoelectron spectroscopy (XPS) (if such equipment is available in the UHV chamber). This sample preparation method has the advantage that it can be used for most types of solid samples. However, in materials which consist of more than one chemical element, different elements might be sputtered with different velocity leading to a non-stoichiometric surface. Annealing metal oxides in UHV often lead to oxygen-deficient samples. Therefore, an additional anneal in oxygen gas is frequently added to the sputter-anneal cycle. However, the highest oxygen pressures that can be used in a conventional UHV chamber without destroying the UHV ($\sim 10^{-5}$ mbar) are sometimes not enough to obtain a stoichiometric oxide.

2.3 Low-energy electron diffraction

Low-energy electron diffraction (LEED) is one of the absolutely most common surface science methods, which is used for determining surface structures. It is based on the fact that moving particles such as electrons can be described as waves with a 'de-Broglie' wavelength of $\lambda = h/mv$ where h is Plancks constant, v is the velocity and m is the mass of the particle. In LEED, a sample is exposed to an electron beam with a variable electron energy in the range 20-500 eV giving a de Broglie wavelength of 2.7-0.5 Å. The de Broglie-wavelength is thus in same length scale as the distance between two atoms in a crystal, which is typically 2-5 Å. The 'electron waves' are thus diffracted at the surface and interferes to form a diffraction pattern that is visualized on a fluorescent screen.

The experimental set-up of LEED is demonstrated in Figure 2.1. An electron gun produces a parallel and monoenergetic electron beam that is focused on the sample. The scattered electrons then pass a system with three grids before it is accelerated onto the fluorescent screen where the diffraction pattern is made visible. Both the sample and the first grid are grounded, so that the scattered electrons can travel in a field free region. A negative potential is applied to the second grid, so that only elastically scattered electrons reaches the fluorescent screen. In order to prevent field inhomogenities in the second grid due to the high potential in the fluorescent screen, a third grid biased with the same potential as the second grid is often placed between the second grid and the fluorescent screen.

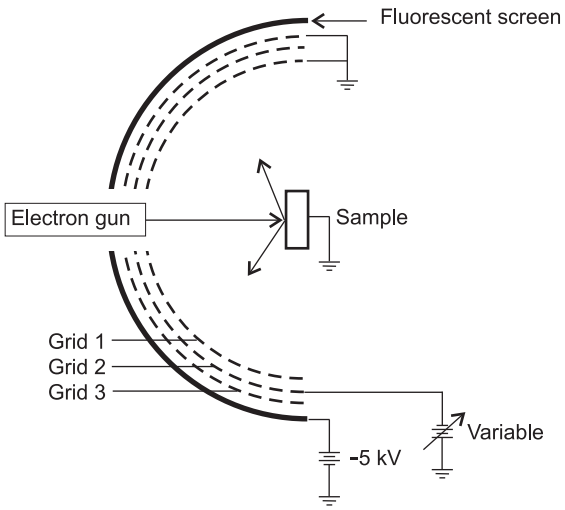

Figure 2.1. LEED experimental set-up

When studying the geometric positions of the diffraction spots, simply by inspection of the LEED pattern, information on the symmetry of the surface structure is obtained. This is normally done as a step in the surface preparation to control the crystallographic quality of the surface and whether the surface is reconstructed or not. In addition, more exact information on the atomic positions in the surface can be obtained by measuring the intensities of the diffracted beams as a function of beam energy (I-V spectra). This is often called structural analysis. Estimations of the atomic positions can then be obtained by comparisons to theoretical calculations. In the work presented here, only simple inspections of LEED patterns have been performed.

A well-ordered surface gives a LEED pattern with small, sharp spots with high contrast and low background. A lot of defects or imperfections in the crystal structure give rise to larger, more diffuse spots. The diffraction pattern can sometimes also give information on what types of imperfections are present in the surface layer of a crystal. An example of this is that arrays of atomic steps on a surface result in spot splitting. Another effect that can be observed in LEED is faceting, i.e. when the crystal surface also contains other crystallographic surfaces, inclined with a small angle to the original surface plane. This results in extra spots in the LEED pattern moving in symmetry directions when changing incident electron energy.

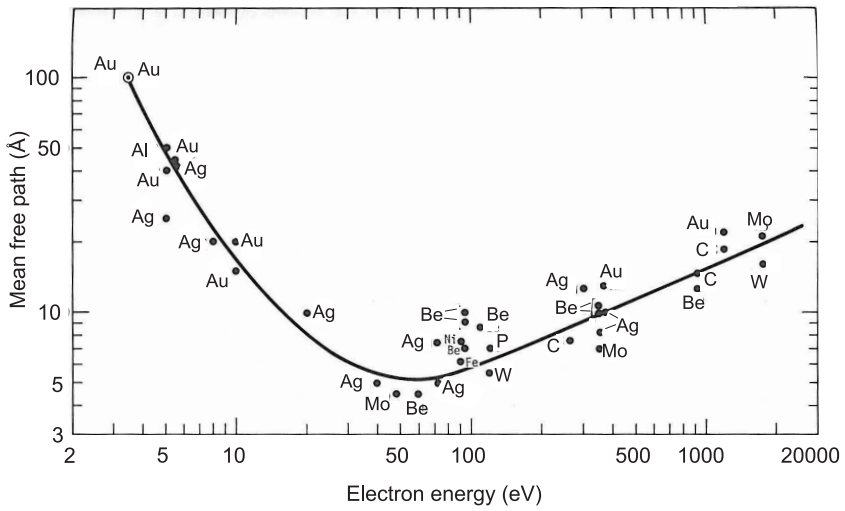

Figure 2.2. Universal curve showing how the mean free path of electrons in various materials depends on the kinetic energy of the electrons. (From [4], fontsize is modified)

2.4 Photoelectron spectroscopy

Photoelectron spectroscopy (PES) is a versatile and powerful experimental technique that is used to study chemical composition, chemical bonding and electronic structure in the surface region of a sample. PES includes several techniques that are based on the photoelectric effect and whose main difference is the type of excitation source. Electron spectroscopy for chemical analysis (ESCA), which was developed by Kai Siegbahn in the 1950:s has later been denoted x-ray photoelectron spectroscopy (XPS). In this technique, x-rays are used as excitation source and mostly core levels are probed. In ultraviolet photoelectron spectroscopy (UPS), the valence band region is studied and ultraviolet radiation is used as excitation source. When using synchrotron radiation, there is no exact border between these two techniques anymore and they are both referred to as PES.

The principle behind PES is the photoelectric effect, i.e. the emission of electrons from a sample upon exposure to light. This effect was initially discovered by Hertz in 1887. In the following years it was found that the kinetic energy of the emitted electrons depends on the frequency of the light and not on the intensity as expected. Einstein later explained the photoelectric effect theoretically by assuming that the electromagnetic radiation is composed of particles or quanta called photons with energy $E_{photon} = h\nu$, where h is Planck's constant and ν is the radiation frequency.

In photoelectron spectroscopy, a sample is exposed to a monochromatic beam of

photons and the intensity of the emitted photoelectrons is then measured as a function of kinetic energy (E_{kin}) in a chosen energy range. The binding energy (E_{bin}) of the electrons in the solid is obtained from the relation $E_{kin} = E_{photon} - E_{bin} - \phi$, where ϕ is the work function of the material. Quantum mechanically, photoemission is a one step process. However to make it easier for the reader to assimilate this process, it is often described by a three-step model. In the first step, a photon is absorbed and an electron is excited to a higher energy level. In the second step, this electron is transported to the surface of the sample. During this process, the electron can be scattered inelastically by e.g. phonons or plasmon excitations. An electron that experienced one single inelastic scattering process contributes to widening or an additional component in the spectrum. If an electron is inelastically scattered more than once, it will contribute to the continuous background in PE spectra. The probability for electron scattering in solids is affected by the kinetic energy of the electron but surprisingly little by the type of solid. This is demonstrated in the 'universal curve' shown in Figure 2.2 where the mean free path of electrons in various materials is plotted as a function of kinetic energy. Continuing with the third step of the model, the electron is emitted from the surface out into the vacuum.

The experimental setup of photoelectron spectroscopy is shown in Figure 2.3. The photon source can be an x-ray tube (XPS), a gas discharge lamp giving ultraviolet light (UPS), a laser source or a synchrotron source. A monochromator (not shown in Figure 2.3) is often used to minimize the energy region of the photon beam in order to improve the resolution in the spectra. Some of the photoelectrons then enter an electron analyser, e.g. a hemispherical analyser, followed by an electron detector.

There are a vast number of different PES techniques not presented here and more are probably to come. Here we focus on core level measurements and angle resolved photoemission.

2.4.1 Core level measurements

PES is used to study the electronic configuration of matter. In solids, the occupied electron levels consist of core levels, i.e. the innermost levels localized on atoms and the valence band. The valence band often consists of a 'mix' of more than one atomic orbitals. Regular core level and valence band photoemission processes are illustrated in Figure 2.4 (a) and (b) respectively. Core levels give information on what elements are present in the surface region of the sample. Although core levels are localized to atoms, their binding energy is changed upon chemical bonding. This phenomenon is called chemical shift and is very useful in determining e.g. the type of bonding and adsorption sites for molecules adsorbed at surfaces. A classical example of chemical shift is the well-known increase of the S $2p$ binding energy for sulfur containing species with the oxidation state of sulfur. The pioneers of such measurements were Hagström et al.[6], who made the first investigations of chemical shifts of different sulfur containing compounds in the 1960:s.

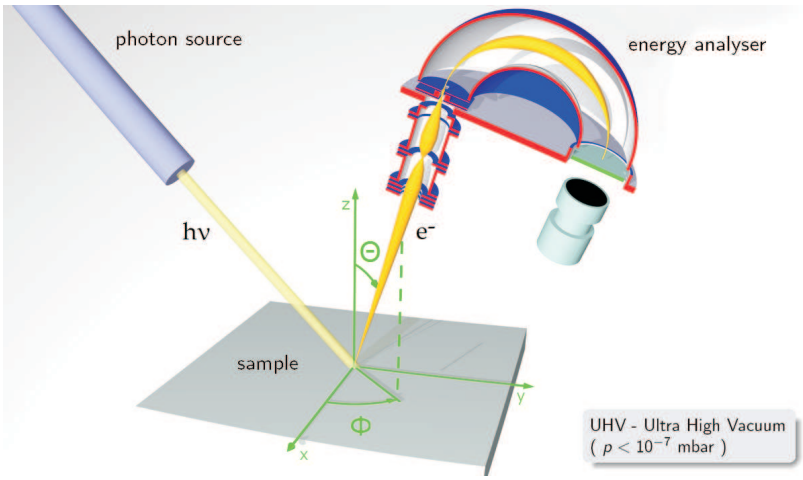

Figure 2.3. Experimental set-up for photoelectron spectroscopy. (From [5])

A spectrum of a core level can contain several components that originate from different groups of atoms having different binding energies. Binding energy shifts can be caused by e.g. chemical shifts, surface shifts or different surface sites. These components can be clearly distinguishable (resolved) or they can lie closely in energy (not resolved). Curve fitting can be used to separate the different components and to get a quantitative estimation of the different contributions. The intention is to obtain a good agreement between a theoretically 'fitted' spectrum with the measured spectrum. This is done by varying a set of parameters to minimize the root mean square (RMS) value of the deviation of the theoretical intensities from the measured intensities in all measured data points. Spectra obtained on semiconductor surfaces are often fitted with Voigt (gaussian-lorentzian) functions. The gaussian width of the spectrum originates from instrumental response, broadening from phonon excitations and chemical and structural inhomogenities. The lorentzian width depends on the core hole lifetime. The other parameters that can be varied are binding energy, spin orbit split and branching ratio. The two latter parameters have theoretically determined values and the fitted values should not differ significantly from these. However, this is sometimes observed due to e.g. diffraction or rapidly varying photoexcitation cross-sections.

When fitting spectra obtained from metals, an asymmetry parameter is introduced giving a 'Doniach-Sunjic' line profile. The reason for the asymmetry of spectra from metals is that when a photoelectron is emitted, it can excite valence electrons into the conduction band, as illustrated in Figure 2.4 (d). This will result in a loss of kinetic energy of the photoelectron and more intensity on the low-kinetic energy or high-binding energy side of the spectrum. In a semiconductor, the same

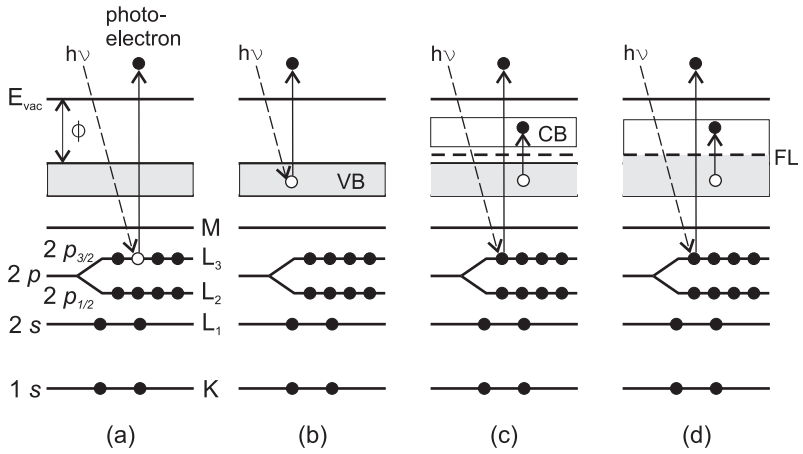

Figure 2.4. Four different photoemission processes

type of secondary excitation will not cause an asymmetry of the spectrum but instead an additional peak, called a shake-up. The reason for this is that valence band electrons in semiconductors demand a minimum addition of energy to be able to excite to the conduction band, namely the energy of the band gap (see Figure 2.4 (c)). Nevertheless, a small asymmetry ($\alpha < 0.035$) of the spectra measured on semiconductor surfaces has been allowed in the curve fittings presented in this thesis, since the agreement were improved upon doing so. The reasons for this assymetry could be assymetric responses from e.g. the analyzer or from phonons. Moreover, unresolved components or a metallic surface on an otherwise semiconducting substrate could also explain asymmetric peaks on semiconductors.

2.4.2 Angle-resolved photoelectron spectroscopy

Angle-resolved photoelectron spectroscopy (ARPES) is one of the most common methods used for studying the valence band electronic structure of solids. In ARPES not only the binding energy of the photoelectrons is recorded but also their emission angles (Θ). If the sample surface is well-ordered and have the same periodicity as the bulk, the electron momentum component parallel to the surface is conserved when a photoelectron is emitted. By using this fact, the $k_{||}$ component in the sample can thus be determined as $k_{||} = \sqrt{\frac{2m_e}{\hbar^2}\epsilon_k}\sin\Theta$, where ϵ_k is the kinetic energy of the electron. This means that band dispersions and charge distributions in Brillouin zones can be obtained from these measurements.

The ARPES measurements presented in this thesis (paper 1) are performed with relatively high photon energies (619 and 891 eV), which are in the soft x-ray regime (200-2000 eV). Normally, ARPES measurements are performed using photon ener-

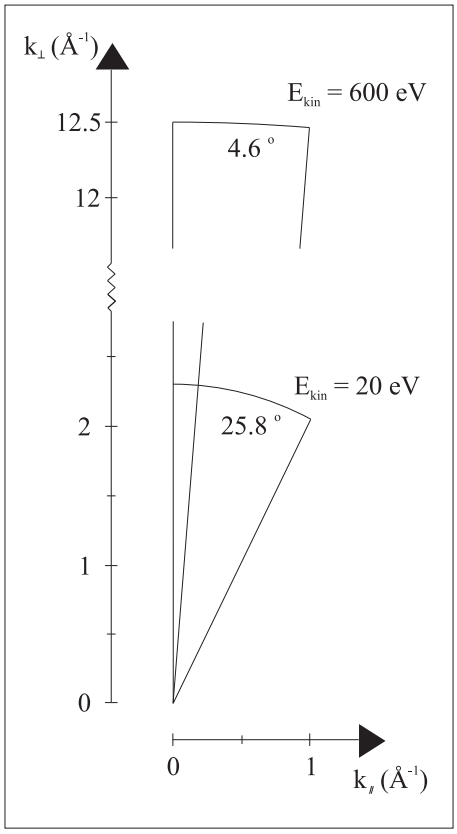

Figure 2.5. Illustration of the path in k-space investigated in a photoemission measurement when keeping photon energy constant and changing the angle. k-space paths for two different kinetic energies for the electrons are shown. (Courtesy of Prof. Oscar Tjernberg)

gies in the energy range, 20-100 eV (UV light), since this normally gives the optimal energy and momentum resolution when using modern synchrotron sources and electron analyzers. Moreover, when using UV radiation, photoionization cross-sections for valence band orbitals are often one order of magnitude higher than when using soft x-rays. There are thus some significant advantages associated with using low photon energies in ARPES. However, there are also some major advantages with using high photon energies. First, when using higher photon energies, the electron mean free path increases and the measurements become more bulk-sensitive. This is favorable for probing the bulk band structure. Another major advantage with higher photon energies is that a smaller range of emission angles is needed to cover a Brillouin zone, as shown in Figure 2.5. As seen in Figure 2.5, a kinetic energy of 600 eV and an emission angle range of 4.6° for the photoelectrons enables measurement along 1 $Å^{-1}$ in the $k_{||}$ direction. Modern angle-resolving analyzers often have an angle of acceptance of ±7°. In Cu_2O, 1 $Å^{-1}$ approximately corresponds to the length of a Brillouin zone in Γ-M direction. A single measurement is therefore enough to measure the band dispersion along the whole Brillouin zone at an energy of 600 eV for this system. In addition, the curvature of the line measured in k-space when using high photon energies is very small, so it can be approximated to be in the $k_{||}$ direction. When using UV radiation, only a small part of the Brillouin zone is covered in one measurement. Moreover, the curvature of the line cannot be neglected and to measure in a straight line in k-space, the photon energy has to be changed for each measurement. Using soft x-rays instead of UV radiation thus simplifies the measurement significantly and also reduces the risks of making mistakes.

2.4.3 Synchrotron radiation

To write about synchrotron radiation in a subsection to photoelectron spectroscopy can be considered misleading, since synchrotron radiation sources are used for a large number of experimental techniques where photoemission is only one of them. Nevertheless, in the work presented in this thesis, it has only been used for photoemission measurements, which motivates the position of this subsection.

In order to obtain PE spectra with high resolution relatively fast, the quality of the photon source is very important. A good photon source is e.g. highly monochromatic and has high photon flux and brilliance. The modern synchrotron radiation sources fulfill all these criteria and it has other advantages such as its tunable photon energy in a wide energy range, linear polarization and pulsed time structure.

The principle behind synchrotron radiation is the well established fact in electromagnetic theory that when a charge is accelerated, it emits radiation. In a synchrotron source, electrons are accelerated in a circular storage ring and some of the emitted radiation is collected and used at the end stations placed around the ring where it is used in experiments. When charge is travelling in a circular orbit with a velocity far below the velocity of light ($v \ll c$), the angular distribution

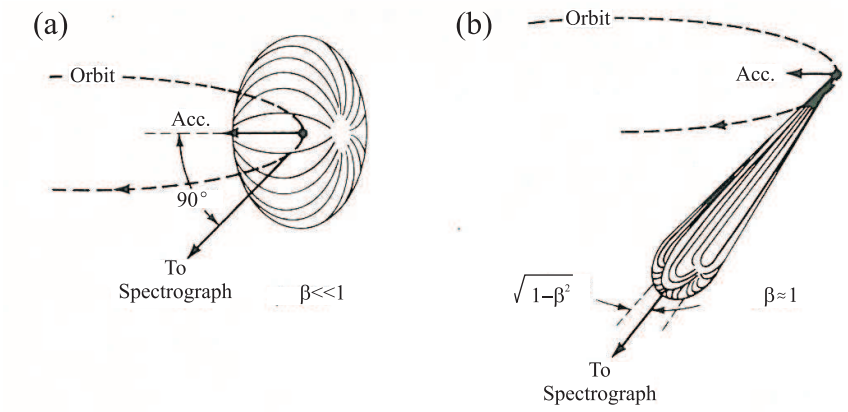

Figure 2.6. Angular distribution of emitted radiation from an electron moving in a circular orbit with nonrelativistic (a) and relativistic ($\beta = v/c \simeq 1$) velocity (b). (From [7])

of the radiation is similar to that of an oscillating dipole and is non-directional as shown in Figure 2.6(a). However, when the charge is moving with relativistic speed (v∼c), as in a storage ring in a synchrotron source, the intensity distribution of the emitted radiation is strongly distorted into a narrow cone directed in the forward direction of the electron motion, as shown in Figure 2.6(b) This radiation has a wide spectral range going from UV to x-rays.

The real storage rings are not perfectly circular but contain straight sections separated by bending magnets. Every time the electrons are accelerated in a bending magnet, they emit radiation that is used in end-stations for experiments. In third generation synchrotron sources, so-called insertion devices, such as undulators and wigglers are often placed in the straight sections of the ring. These devices contain periodic arrays of magnets, which bend the electron beam back and forth giving a wavelike trajectory. An insertion device enables higher photon flux and brilliance than a bending magnet.

The ARPES measurements presented in paper 1 were performed at the BL25SU end station at SPring-8 in Japan. The other PES measurements presented in papers 3, 4, 5 and 6 have all been performed at beamline I511-S at MAX-lab in Sweden. Both beamlines are undulator-based.

2.5 Scanning tunneling microscopy

The scanning tunneling microscope was first developed in 1981 by Binning and Rohrer at IBM in Zürich. In 1986 they obtained the Nobel Price in physics for this achievement. Scanning tunneling microscopy (STM) can give images with lateral

and vertical resolutions of ~ 2 Å and 0.01 Å respectively, which enables probing and control of individual atoms. This microscope can be used in various environments such as atmospheric and UHV conditions and the sample can even be immersed in liquid. In addition, tunneling is possible in a wide temperature range, from near zero Kelvin up to several hundred Kelvins.

The principle behind STM is quantum mechanical tunneling, i.e. the effect when electrons with energy E penetrate an energy barrier with energy $\Phi > E$. This effect is forbidden in classical physics but in quantum mechanics, the electrons are represented by wave functions which damps out but don't disappear completely outside barriers with energy $\Phi > E$. In the scanning tunneling microscope, tunneling is enabled by applying a bias voltage between the sample and an atomically sharp metallic tip that is brought very close (within a few Å) to the sample. The tunneling current I_T depends exponentially on the distance d between tip and sample as $I_T \propto e^{-2kd}$ where $k = \sqrt{2m(\Phi - E)/\hbar^2}$ and m is the electron mass [8]. The tunneling current is thus very sensitive to a change in d and this is the effect that enables topographic measurements at the atomic scale with STM. Generally, a change in d of 1 Å gives a change in current of one order of magnitude.

In Figure 2.7, the experimental setup of an STM is shown. The first sample to tip approach is made by a coarse sample to tip control (not shown in Figure 2.7). Scanning the sample in lateral (x,y) direction and fine adjustment in vertical (z) direction is controlled by piezoelectric scanners. The tunneling current is measured and amplified and this signal is used in a feedback loop in order to regulate the voltages applied to the piezoelectric devices that keep a constant current. This is called constant current imaging (CCI). If the surface is very flat, the feedback loop can be turned off to measure the current changes during scanning and this is called constant height imaging (CHI) or variable current mode. The latter mode enables much faster scanning. Since the current is very sensitive to the vertical position of the tip, vibrations will highly effect the measurements. Typically, vibrations in buildings can come from large low-frequency movements of the building, running machines, ventilation, motors, people moving and acoustic noise [8]. To get a stable microscope, an efficient vibration isolation system is thus needed. For highest possible stability, the STM should be placed in the basement and the whole UHV system should be mounted on e.g. pneumatic legs. A commonly used damping system used inside the UHV system is one where the STM is mounted on a two-stage spring system with eddy-current damping (see Ref.[8]) and the sample is placed on a stack of metal plates alternated with Viton rings.

Although STM gives local information at the atomic scale, it does not always show the real position of the atoms. When using the constant current imaging mode, the tip movement that occurs to retain a constant current is what is giving the image. It is thus the surface charge density of mobile electrons close to the Fermi level that is probed. When tunneling from the tip into the sample, unoccupied states are probed while occupied states in the valence band are probed when tunneling in the opposite direction. This is, however, not the whole truth since the geometric and electronic structure of the tip influence the measurement more or less. What

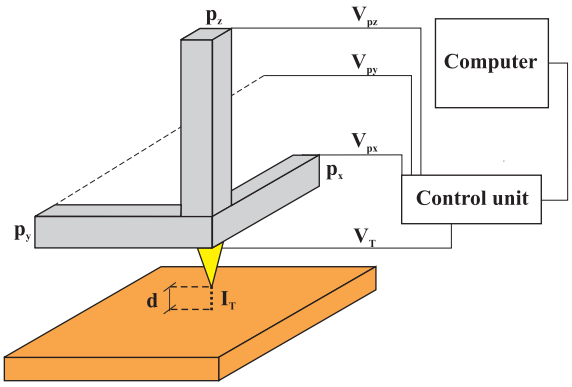

Figure 2.7. STM experimental set-up

we see in the image is thus a convolution of the geometric and electronic structure of both the sample and the tip [9].

By sweaping the tunneling bias and measuring the current in every point in an image, information about the electronic structure around the Fermi level can be obtained. This is called scanning tunneling spectroscopy (STS). In STS, as well as in STM, one should be aware of that the tip electronic structure can highly influence the measurement.

The STM measurements performed in the work presented in this thesis have been made at room temperature with a variable-temperature Omicron STM.

Chapter 3

Metal oxides

Background, results and discussion

Metal oxides are widely used materials in various applications such as electric components, building materials and refractories in e.g. furnaces. Moreover, at atmospheric or high pressure (e.g. in chemical reactors) conditions, most metals are covered with an oxide layer and it is this oxide layer that interacts with the surrounding atmosphere. Studies of metal oxide surface properties are thus of great importance to get a better understanding of corrosion of metals, heterogeneous catalysis and gas sensors. Although the majority of the work presented in this thesis concerns metal oxide surfaces, a considerable part of this chapter will treat bulk properties. This is motivated by the fact that bulk and surface properties are intimately linked and to get a good understanding of a surface, both bulk, surface and interactions between them have to be considered.

Among metal oxides, there is one very technologically important group of materials, namely the transition metal oxides. These materials have extremely varied electric properties, ranging from isolating to metallic and exhibits several interesting phenomena such as superconductivity and metal-insulator transitions. Transition metals are metals with an unfilled d shell in their electronic configuration. A common characteristic of these materials is the existence of several oxidation states of transition metal ions which can convert to one another. Iron can e.g. have two different oxidation states (+II and +III) while vanadium can have as many as four states (+II, +III, +IV and +V). This explains why two or more types of oxides often can be obtained from one type of transition metal. The ability of transition metal cations to change oxidation states can explain many of the interesting properties of transition metal oxides. In the present study, the studied oxides are Cu_2O, Fe_3O_4 and ZnO, where the first two are transition metal oxides. Even though zinc is often included in the group of transition metals or post-transition metals, zinc cations do not easily change oxidation number, since the only stable oxidation number for a zinc cation is +II.

Most metal oxides in technologically important applications are used in the form of polycrystalline powder or in polycrystalline or crystalline ceramic form [10]. Amorphous oxides are relatively uncommon [10]. This means that all exposed surfaces are different crystalline surface terminations. Thus, when making experimental studies on surface properties and reactions on a fundamental level, single crystalline samples are required. A single crystalline surface can either have the same structure as the crystallographic plane in the bulk or it can be reconstructed. The driving force for reconstruction is minimization of the Gibbs free energy per unit surface area. Generally, surfaces with a smaller number of broken bonds are more stable. Since oxides contain positively charged metal cations and negatively charged oxygen anions, an atomic plane can, e.g. if it contains only one type of ion have a net charge. The surface associated with this type of plane is called a polar surface, but these surfaces are not constructed as in the bulk due to instability. Instead the surface is stabilized by (i) charge transfer between the two opposite polar surfaces, (ii) formation of surface ion vacancies, which can lead to a change of the geometric positions of the surface ions, and (iii) adsorption of charged species such as OH^- ions.

The density and types of defects are always central issues when trying to understand both bulk and surface properties of metal oxides. A change in defect concentration can give large changes in e.g. conductivity, color and chemical properties. Common defects are point defects or line defects such as dislocations in the bulk or steps on surfaces. In metal oxides, an abundant and important group of defects are due to nonstoichiometry of the crystal. This gives defects such as cation or anion vacancies and interstitials. Many of the interesting properties of transition metal oxides are caused by nonstoichiometry. For example, the superconductivity of cuprates has been shown to be strongly coupled to the number of oxygen vacancies. The defect density is often higher on surfaces than in the bulk and defects often govern the catalytic or chemical properties of an oxide surface. The difference between defect sites and regular surface sites is generally larger on an oxide surface than on e.g. a metal surface.

The metal oxides and surface terminations, which are the subject of this thesis will shortly be introduced below. An important reason to study these materials, is that they are formed on metal surfaces at ambient conditions. Therefore, every section below begins with a description of the role of every particular oxide in the initial atmospheric corrosion process.

3.1 Cuprous oxide

The atmospheric corrosion of copper starts with the formation of at least two layers, which both contains Cu^{2+} cations. The layer closest to the metal contain cuprous oxide (Cu_2O) and the outer layer contains bound water, hydroxyl and carbon. Cu_2O is by far the most common corrosion product and represents about half of the total mass of the patina layer formed upon corrosion of copper [11]. This might

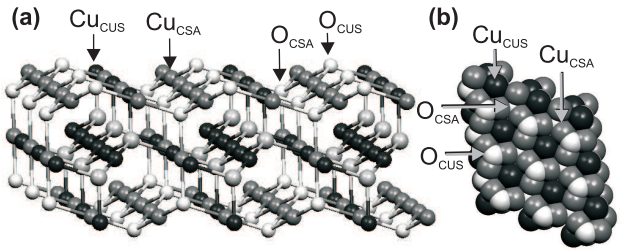

Figure 3.1. (a) Side view of a stick and ball model of the ideal bulk-terminated $Cu_2O(111)$ surface. (b) Top view of the model shown in (a) but with a space-fill model. In the topmost sublattice, copper and oxygen ions are grey and white respectively. In the second sublattice, copper ions appear black and oxygen ions have a light grey color.

also explain why it is the major ore of copper.

Cu_2O and/or Cu^+ ions have been shown to play important roles in copper-based catalysts [12, 13]. Moreover, potential future applications for this oxide are found in solar energy conversion [14] and photocatalytic splitting of water [15].

Cu_2O is a p-type semiconductor with a band gap of 2.2 eV [16, 17]. The p-type doping is mostly caused by copper vacancies [18]. The crystal structure of Cu_2O consists of two interpenetrated and independent cristobalitelike lattices as seen in Figure 3.1 (a). Another way of describing this structure is that oxygen anions form a bcc lattice and every oxygen anion is surrounded by a tetrahedron of copper cations. The Cu_2O structure contains unusual O-Cu-O bonds that also are present in the CuO_2 planes in high-T_c cuprate superconductors. Thus, even though Cu_2O is not superconducting, detailed studies of this material can lead to a better understanding of high-T_c superconducting cuprate materials.

3.1.1 Cu_2O electronic structure

The electronic structure of Cu_2O has been the subject of a large amount of experimental as well as theoretical studies. A subject that has been thoroughly discussed and debated is the charge distribution and bonding in Cu_2O. In the simple ionic model, Cu_2O has a 3 d^{10} configuration giving spherically symmetric Cu^+ and O^{2-} ions and ionic bonds. However, many studies indicate that the short Cu-Cu and O-O distances and the linear O-Cu-O bonds found in Cu_2O would be unstable in the case of complete ionization. There are several studies, which confirm that the charge density around copper ions is not fully spherical [19–25]. The non-spherical charge distribution around copper cations could be due to an intra-atomic Cu 3d-Cu 4 sp hybridization, which has been predicted in many studies [22, 25–30]. However, it is not clear whether this hybridization is close to negligible or if it has a substantial impact on the bonding in the material.

The valence band structure of Cu_2O has been studied both theoretically with various band structure calculations and experimentally, mostly with PES. Two main regions with bands of mainly Cu $3d$ and O $2p$ character respectively have been identified in the valence band. In between these two regions, a dispersive band of Cu $3d$-$4s$ character has been predicted theoretically but was never confirmed in a photoemission spectrum in the literature until the study in paper 1 was published. Bruneval made a study of orbital characters of different bands in the Cu_2O band structure [28]. In this study, the mixed Cu $3d$-$4s$ band was predicted to have a character that is 60% Cu $4s$ and 36% Cu $3d$ at the Γ-point. Since this band is highly dispersive, it is hard to distinguish it in normal PES spectra and therefore ARPES measurements would be more appropriate in this case. Bruneval et al. [31] made ARPES measurements but did not resolve the predicted Cu $3d$-$4s$ band.

Cu_2O electronic structure: Results and discussion

The ARPES study on the bulk electronic structure of Cu_2O that is presented in paper 1 is the only one of its kind in this thesis. A comparison between this study and the studies in papers 2 and 3 concerning the $Cu_2O(111)$ surface can thus be a bit far-fetched. The electronic structure of the bulk is of course intimately linked to that of the surface. However, no studies on e.g. surface states on $Cu_2O(111)$ are presented in this thesis, although such a study would be highly relevant. Therefore the results and discussion on paper 1 are presented very shortly here and the reader is referred to the summary of papers in chapter 5.

The only other ARPES measurement proceeding the one presented in paper 1 was made by Bruneval et al., who investigated the bands along the Γ-R direction using low-energy ARPES. In order to get an improved picture on the valence band structure of Cu_2O, we have investigated the Γ-M direction by means of high-energy ARPES. As described in section 2.4.2, there are many advantages with using high photon energies and this together with an efficient background subtraction has given a more clear picture of the bulk valence band structure of Cu_2O. Moreover, the dispersive hybridized Cu $3d$-$4s$ band was resolved experimentally for the first time.

3.1.2 $Cu_2O(111)$

$Cu_2O(111)$ is an imperfect cleavage plane of cuprous oxide, meaning that cleaving leaves a surface that is dominated by the (111) plane. It has also been reported to be the most common surface in Cu_2O polycrystalline films [32], microcrystals [33] and nanocrystals [34]. Moreover a $Cu_2O(111)$-like surface structure can be formed under certain conditions upon oxygen adsorption on Cu(111) [35–38].

Since the cuprous oxide crystal consists of O-Cu-O sandwiches, stacked in the [111] direction (O-Cu-O - O-Cu-O), the bulk-terminated $Cu_2O(111)$ surface can be both oxygen- and copper-terminated. Copper-termination gives a polar surface that has been shown to be less stable than the oxygen-terminated nonpolar surface

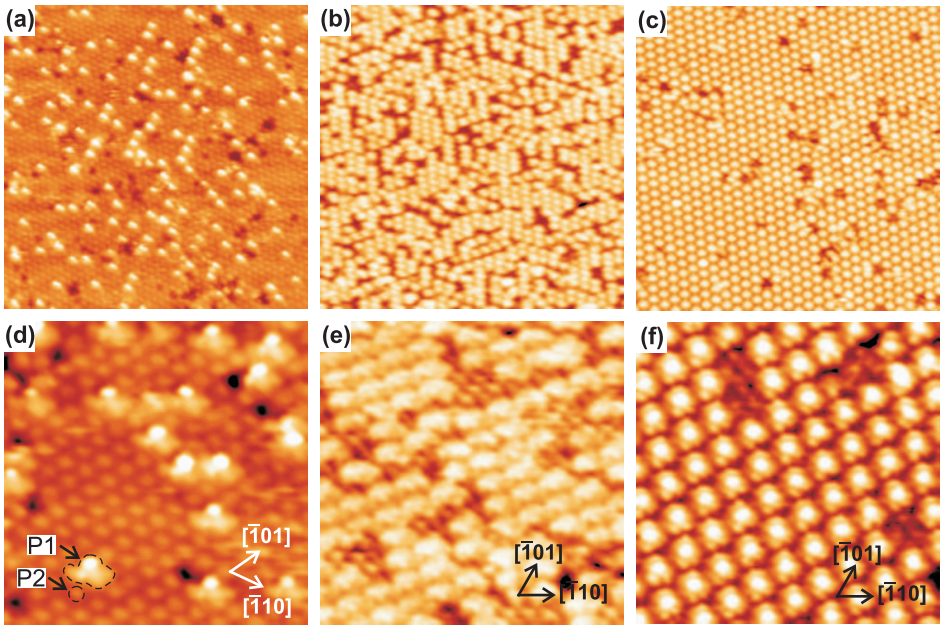

Figure 3.2. 300 Å x 300 Å ((a)-(c)) and 100 Å x 100 Å ((d)-(f)) STM images of clean $Cu_2O(111)$ surfaces. Tunneling parameters are (-1.0 V, 0.3 nA) for (a) and (d), (-2.5 V, 0.2 nA) for (b), (-2.0 V, 0.1 nA) for (c), (-1.0 V, 0.2 nA) for (e) and (-0.75 V, 0.05 nA) for (f). Two different types of protrusions (P1 and P2) are marked out in (d) and crystallographic directions are illustrated in (d)-(f). (From paper 3 in this thesis)

[39]. The oxygen-terminated $Cu_2O(111)$ structure contains four different surface sites, namely coordinatively saturated copper and oxygen ions (Cu_{CSA} and O_{CSA}) and coordinatively unsaturated ions (Cu_{CUS} and O_{CUS}) as shown in Figure 3.1 (b) and (c). The exact atomic structure of $Cu_2O(111)$ has been the subject of several recent theoretical studies [12, 39, 40]. Soon et al. and Li et al. have shown that the most stable surface configuration of $Cu_2O(111)$ is one where Cu_{CUS} cations are missing, called the $Cu_2O(111)$-Cu_{CUS} surface. This was found to be the preferred termination in a wide range of oxygen chemical potentials including UHV conditions.

$Cu_2O(111)$: Results and discussion

The clean $Cu_2O(111)$ surface structure is treated in both papers 2 and 3. Paper 3 also involves adsorption studies that of course are interesting in a chemical point of view. In addition to this, the molecules can serve as probe molecules, giving a better view of the adsorption sites and defects on the surface.

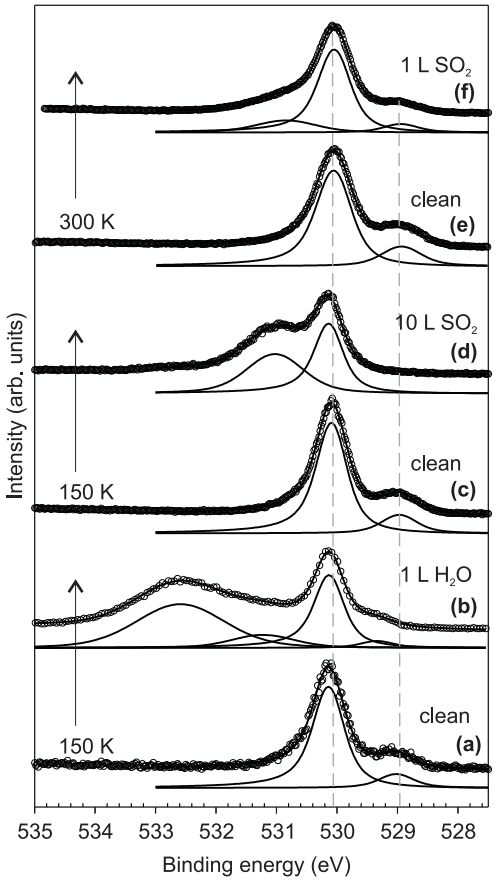

Figure 3.3. O 1*s* core level spectra ($h\nu$=670 eV) from $Cu_2O(111)$, before and after exposure to water and sulfur dioxide.

In paper 2, an attempt was made to get information about the exact atomic structure of the $Cu_2O(111)$ surface and in particular whether the $Cu_2O(111)$-Cu_{CUS} surface model, suggested by Soon et al. [12, 40] is valid. This was done by comparing STM images of a $(\sqrt{3} \times \sqrt{3})$R30° reconstructed surface and a (1x1)-dominated region with two surface models. Unfortunately, no reliable information on whether the Cu_{CUS} cations are missing or not was obtained. However, our studies revealed interesting information about surface defects, which is presented below.

We have discovered that when preparing the $Cu_2O(111)$ sample by sputtering and annealing in UHV, a $(\sqrt{3} \times \sqrt{3})$R30° LEED pattern is obtained. The reconstructed surface gives STM images that are dominated by large protrusions, called

P1, as shown in Figure 3.2 (c) and (f), arranged in a $(\sqrt{3} \times \sqrt{3})$R30° structure. At some spots, P1 are missing and in these spots, smaller protrusions, called P2 are visible. The P2 protrusions are ordered and form a (1x1) pattern. When preparing the sample by sputtering and annealing in oxygen ($2 \cdot 10^{-6}$ mbar), a (1x1) LEED pattern is obtained. The STM images show a surface dominated by P2 protrusions, forming a (1x1) pattern, as shown in Figure 3.2 (a) and (d). P1 protrusions are also present on the (1x1)-terminated surface but in an unordered fashion. After many sputter and anneal (in oxygen) cycles, weak $(\sqrt{3} \times \sqrt{3})$R30° spots appear in the LEED pattern and P1 protrusions are more numerous and more ordered, as shown in Figure 3.2 (b) and (e). Since the reconstructed surface is obtained when annealing in UHV, we suggest that the reconstruction is based on oxygen vacancies, in accordance with the conclusions of an earlier study on the $Cu_2O(111)$ surface [41]. Another interesting point was that the LEED pattern from the reconstructed surface also showed additional spots moving in the symmetry direction when changing photon energy, which is a sign of surface faceting and island formation. When obtaining a (1x1) LEED pattern, however, no extra spots were observed. This indicates that island formation and faceting is linked to the oxygen deficiency of the crystal.

In all O 1s spectra from clean $Cu_2O(111)$ surfaces, there are two components that are clearly resolved. The main peak is located at a binding energy of 530.0-530.1 eV. Another peak is located at 528.9-529.0 eV and is shifted with 1.1-1.2 eV from the main peak. The peak area of the latter component is around 15-24% of the area of the main component. It is shown to at least partly be represented by surface oxygen anions. The peak could not represent all surface oxygens due to its small relative size to the main component. When looking at the STM images in Figure 3.2 (a) and (d), there are two types of defects that are clearly visible, i.e. the P1 protrusions representing oxygen vacancies and dark pits, which probably represent one or several copper vacancies. The copper vacancies have a surface density of $\sim$5% and are more probable to be related to the low BE peak. This suggests that the low BE peak could be represented by oxygen anions close to copper vacancies, giving rise to oxygen anions with more than one broken bond (O_{MCUS}). The index MCUS stands for 'multiply coordinatively unsaturated'. This assignment is confirmed by the study by Harmer et al. [42], who observed a similar component in their studies of fractured $Cu_2O(111)$ surfaces and assigned it to undercoordinated oxygen anions.

By adsorbing water and sulfur dioxide on (1x1)-dominated $Cu_2O(111)$ surfaces, it was discovered that the O_{MCUS} anions probably could be divided into at least two groups. In Figure 3.3, the evolution of the O 1s spectrum upon adsorption of water at 150 K ((a)-(b)) and sulfur dioxide at 150 K ((c)-(d)) and at 300 K ((e)-(f)). When H_2O is adsorbed at 150 K, the O_{MCUS} peak decreased in size. The same thing happens upon SO_2 adsorption at room temperature. Moreover, the relative size of the O_{MCUS} peak is about the same upon SO_2 adsorption at room temperature as after adsorption of 1 L H_2O. This indicates the presence of two or more different groups of O_{MCUS} anions on $Cu_2O(111)$. When SO_2 is adsorbed at

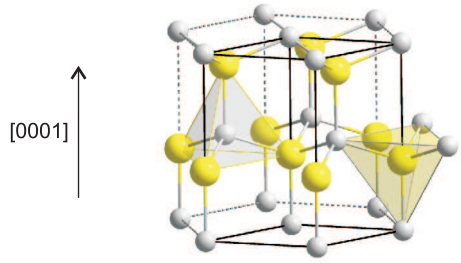

Figure 3.4. Wurtzite crystal structure. Zinc ions are small and white and oxygen ions are large and yellow. (From [44])

150 K, the O_{MCUS} peak disappears totally. This other group of O_{MCUS} anions thus have a lower reactivity towards both water and SO_2 and this will be treated further in the section on SO_2 adsorption 4.2.1.

3.2 Zinc oxide

Zinc is well known for its use in corrosion protecting layers on steel (galvanization). At atmospheric conditions, zinc reacts immediately with air to form zinc oxide and when water is present, zinc hydroxide [1]. A protective film of zinc carbonate is then formed [1]. This layer is only stable in a small pH range and gaseous pollutants such as sulfur dioxide or particles that acidify the water layer covering the surface can highly influence the degradation of zinc.

In form of a powder, ZnO is used as an additive in a large range of materials and products, e.g. rubber and pigments. Moreover, the interest in zinc oxide as a material for new potential applications has got a recent upswing, mostly because of its semiconducting and optical properties. Zinc oxide surfaces are very useful in catalysis and gas sensing. One of the most important technological applications of zinc oxide surfaces is in the chemical industry, where $Cu/ZnO/Al_2O_3$ catalysts are used in e.g. methanol synthesis [43].

The most common crystal structure of ZnO is wurtzite, shown in Figure 3.4. Zinc oxide is a semiconductor with a direct band gap of 3.4 eV [10] and has intrinsic n-doping. The cause of this doping has been under discussion. The three most common point defects, which also have lowest formation energies are oxygen vacancies, zinc interstitials and zinc vacancies [45]. However, both theoretical and studies have shown that these defects could not explain the n-type doping in ZnO [45]. On the other hand, hydrogen has shown to be at least partly responsible for the n-type doping in ZnO crystals [46]. Several types of hydrogen have been found, e.g. H bound in an oxygen vacancy (H_O) [47], H incorporated in the crystal at the Zn-O bond centered site (H_{BC}) [47], two hydrogen species bound to a zinc vacancy

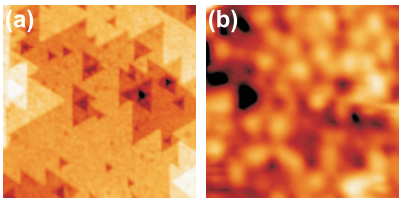

Figure 3.5. 500 Å x 500 Å (a) and 100 Å x 100 Å (b) STM images of the clean ZnO(0001) surface obtained with tunneling parameters (3.0 V, 0.04 nA).

($V_{Zn}H_2$) [48] and H_2 complexes or so-called 'hidden hydrogen' [49, 50]. Both H_O and H_{BC} have been identified as n-type donors [47].

3.2.1 ZnO(0001)

Even though ZnO(0001) and ZnO(000$\bar{1}$) are polar surfaces they appear to be the second most common type of surfaces in ZnO powders. Moreover, the understanding of the polar surfaces of ZnO is much less developed than that of the stepped ZnO(10$\bar{1}$0) surface, which is the most energetically favorable ZnO surface [51]. Consequently, there is a need for more fundamental studies on the polar ZnO surfaces in order to get a better understanding of the chemical properties of e.g. ZnO powders and nanoparticles.

In the [0001] direction, wurtzite ZnO consists of zinc and oxygen layers. A ZnO crystal cut in the (0001) plane is thus zinc-terminated (ZnO(0001)) on one side and oxygen-terminated (ZnO(000$\bar{1}$)) on the opposite side. In this thesis, only the zinc-terminated surface has been studied, although a comparison to the oxygen-terminated surface would have been interesting. It has been shown that this polar surface can be stabilized with different mechanisms depending on sample preparation and ambient conditions. Stabilization mechanisms that have been observed are various reconstructions [52–55], adsorption of atoms or molecules [54–58] and an electron accumulation layer caused by surface donors [59].

ZnO(0001): Results and discussion

The band gap of ZnO is quite large and the low conductivity of ZnO samples thus makes STM measurements difficult. Atomically resolved STM images have been obtained from the ZnO(10$\bar{1}$0) surface but not from any of the polar ZnO surfaces, at least not in my knowledge. The STM images of the clean ZnO(0001) surface shown in paper 4 and in Figure 3.5 are of the same quality as earlier published STM data [52]. The surface structure with triangular islands and pits is typical for samples annealed at temperatures of 600-700 °C in UHV. When zooming in on a terrace, it is shown to be covered with relatively large protrusions (10-15 Å) that have an uneven distribution on the surface. Ostendorf et al. [53] have observed

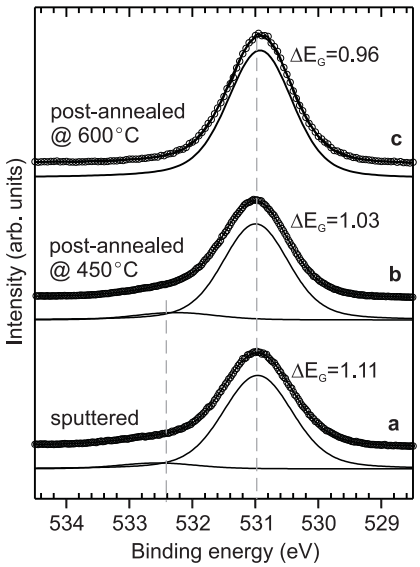

Figure 3.6. O 1*s* core level spectra ($h\nu$=619 eV) from clean ZnO(0001) surfaces.

these features in an AFM study of ZnO(0001) but they did not comment on their possible origin. We have suggested that these features could be triangles, whose shape is too small to be resolved with the tip used. However, we have no evidence for this and further studies of these protrusions are needed.

The effects of sample preparation on ZnO(0001) have been investigated with PES. Annealing is shown to lead to oxygen deficiency in the sample and this effect increases with annealing temperature as shown in valence band spectra (see Fig. 5 in paper 5). Higher annealing temperature also leads to a more well-ordered surface, as evidenced by a more distinct LEED pattern and a narrow O 1*s* line. An annealing temperature of 600-650°C gives an optimal LEED pattern and a well-ordered surface as shown in STM images. At this temperature, hydrogen bound to oxygen also disappears from the crystal. This is shown in the O 1*s* spectra in Figure 3.6. All O 1*s* spectra have a main peak at 529.9-530.0 eV attributed to oxygen in the oxide. At ∼532.3 eV, a peak assigned to hydroxyl groups is present in the spectra from all studied surfaces (sputtered only and sputtered and annealed at 450 and 530°C) except for the one annealed at 600-650°C.

At a first glance, one would expect that the sample surface annealed at highest temperature would give the most conductive sample. A higher annealing temperature will give more defects related to oxygen deficiency, which contributes to the n-type doping found in ZnO samples. However, at the same time, different types of hydrogen leave the sample at certain temperatures and since some types of hy-

drogen serve as dopants in ZnO, a higher annealing temperature could also lead to lower conductivity. This effect might have been observed by the present group, though indirectly, namely through the adsorption of SO_2. When trying to measure S $2p$ spectra on SO_2 exposed ZnO(0001) surfaces, serious charging problems were experienced but only with samples that had been annealed at 600-650°C. This could be due to that these samples were less conductive, although another explanation treated in section 4.2.1 could also be valid.

3.3 Magnetite

In the initial atmospheric corrosion of iron, a rust layer consisting of various forms of iron oxides, e.g. magnetite (Fe_3O_4) and iron oxyhydroxides is formed [1]. Magnetite is also one of the most important ores of iron. Moreover, it is used as a catalyst in technologically important reactions such as the Fischer Tropsch synthesis and the water gas shift reaction [60].

Magnetite has an inverse spinel crystal structure with Fe^{2+} ions at octahedral sites (called B sites) and an equal amount of Fe^{2+} and Fe^{3+} ions at tetrahedral (A) sites. The mixed valency in magnetite, enables charge transfer between Fe^{2+} and Fe^{3+} ions which gives rise to several interesting properties of this material. Verwey et al. found that magnetite undergoes a transition below ∼120 K where the electrical conductivity changes abruptly by two orders of magnitude [61]. This is accompanied with a change in crystal structure. Although the Verwey transition has been studied for more than 80 years, its nature and origin are still debated. Another interesting property of magnetite is that it is ferrimagnetic with an unusually high critical temperature of ∼860 K. This, together with its half-metallicity at room temperature makes it a good candidate for spintronic applications.

3.3.1 Fe_3O_4(100)

Even though Fe_3O_4(100) is not the most commonly occurring surface it is probably the most well-studied surface of magnetite. Two different bulk truncations of the (100) surface of Fe_3O_4 are possible. Either it is terminated by A layers containing tetrahedral iron cations or by B layers that consist of octahedral iron and oxygen ions. Both of these surfaces are polar and must thus be stabilized by any of the three mechanisms earlier described in the introduction to this chapter. A $(\sqrt{2} \times \sqrt{2})$R45° reconstruction of Fe_3O_4(100) has been observed experimentally [62–64]. Various models for the atomic structure of the reconstructed surface have been suggested, e.g. an A layer with half of the tetrahedral irons missing [62] and B-termination with oxygen vacancies [63, 65]. However, the latest and most promising model of the reconstructed surface is found in a combined DFT/LEED study by Pentcheva et al. [64, 66]. They suggest that the reconstruction is the result of a Jahn-Teller distortion. The original Jahn-Teller theorem states that a non-linear molecule that has a degenerate electronic ground state will distort in order to lower its symmetry and remove the degeneracy [67]. In Fe_3O_4(100), the result of such a distortion

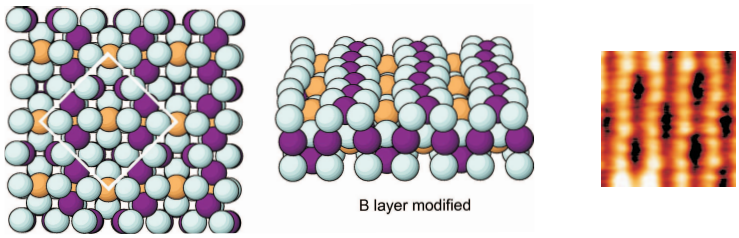

Figure 3.7. Top (a) and side (b) views of stick and ball models of the $(\sqrt{2}\times\sqrt{2})$R45° reconstructed $Fe_3O_4(100)$ surface, where the reconstruction is the result of a Jahn-Teller distortion [64]. Oxygen, FeA and FeB ions are marked with cyan, orange and purple circles respectively. A 33 Å x 33 Å STM image of the clean $Fe_3O_4(100)$ surface with tunneling parameters (1.1 V, 0.3 nA) is shown in (c). ((a) and (b) are taken from [64]: Courtesy of Dr. R. Pentcheva)

would according to Pentcheva et al. [64] be a wave-like structure along the [110] direction giving a $(\sqrt{2}\times\sqrt{2})$R45° reconstruction as shown in the surface model in Figure 3.7 (a) and (b). In Figure 3.7 (c), an STM image of the $(\sqrt{2}\times\sqrt{2})$R45° reconstructed $Fe_3O_4(100)$ surface is shown. The bright features are represented by Fe B cations and the wave-like structure is clearly seen in the image.

Chapter 4

Molecular interactions with oxide surfaces

Background, results and discussion

This chapter is devoted to the interaction of gaseous molecules with solid metal oxide surfaces. It should be noted that solid-liquid interfaces are just as important in e.g. corrosion processes. Due to instrumental difficulties, the understanding of solid-liquid interfaces at an atomic level is lagging behind that of solid-gas interfaces. By the use of methods such as electrochemical STM and sum-frequency generation spectroscopy (SFG), this field is however currently under strong development.

Two types of solid-gas adsorption mechanisms can be distinguished, namely physisorption and chemisorption and typical potentials for these mechanisms are shown in Figure 4.1. This figure describes the potential a hydrogen molecule 'feels' when approaching a metal surface.

In physisorption, the adsorbed entity called the adsorbate is bound to the substrate rather weakly with something similar to the van der Waals force in molecular physics and the electronic structure of the adsorbate is almost intact. The van der Waals force between two atoms or molecules is caused by correlated charge fluctuations in the atoms or molecules, i.e. the force is between two point dipoles. When the latter type of force is between a molecule and a surface, the situation is somewhat different and this force can be called an 'image-charge' attraction [3]. Physisorption is characterized by low binding energies on the order of 10 to 100 meV and large equilibrium separation of 3-10 Å [3].

In chemisorption, a strong chemical bond (covalent or ionic) is formed and the electronic structure of both adsorbate and substrate are strongly influenced. Chemisorption implies high binding energies on the order of a couple of eV and short equilibrium separation (1-3) Å [3]. Most of the electronic interaction occurs by electron transfer from an occupied state of the substrate into the lowest unoccupied molecular orbital (LUMO) of the molecule and from the highest occupied molecular orbital (HOMO) of the molecule to an unoccupied state of the substrate. Chemisorption of molecules can lead to dissociation and formation of new adsorbate

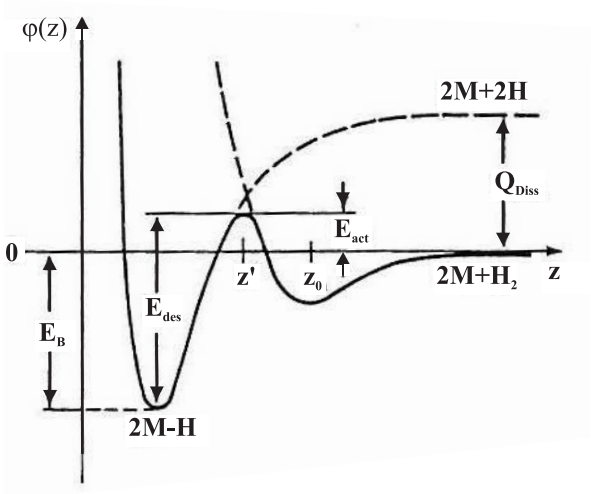

Figure 4.1. Combination of a physisorption and a chemisorption potential for adsorption and dissociation of a H_2 molecule on a metal (M) surface. Q_{Diss}, E_{act}, E_{des} and E_B are symbols for dissociation energy, activation energy for dissociation, desorption energy and binding energy respectively. (From [3])

species. Therefore chemisorption of molecules can be divided into the two groups (i) *molecular* and (ii) *dissociative*.

Mutual adsorbate interactions are of large importance for e.g. the structure of the adsorbate layer and for surface chemistry. The most important types of adsorbate-adsorbate interactions are the *van der Waals attraction*, *dipole forces* between polar molecules such as H_2O or NH_3 giving rise to repulsive forces when the dipoles are parallel, repulsive interaction due to *orbital overlap* between adsorbates when they are packed densely together and *substrate mediated interactions*. The last type of interaction typically appears when a molecule adsorbs and attracts or donates electrons to the surface and thus changes the surface electronic structure around the adsorption site. This will in its turn influence the adsorption of another molecule at these sites. Adsorbate-adsorbate interactions are much more significant when the coverage is around one monolayer than if it is just a fraction of a monolayer. Also the surface chemistry can be largely coverage dependant and this is important to have in mind when doing surface science experiments.

In the chemical point of view, studies of chemisorption under well controlled conditions are of course an excellent method to understand chemical reactions at a fundamental level. However, one should be careful when trying to apply knowledge gained from experiments performed at UHV conditions directly to reactions in corrosion or catalysis. These reactions involve pressures equal to or higher than atmospheric pressures. A higher pressure mostly results in a larger number of sur-

face reactions per time unit and higher adsorbate coverage. As already mentioned, a higher coverage can have large influence on surface chemistry. Moreover, if a surface reaction takes place at defect sites with very low surface density, the small coverage at UHV conditions can result in problems with detecting the small amount of chemical reaction products formed. One way to simulate the chemistry at higher pressures with experiments performed at UHV is to lower the temperature to below room temperature. This will increase the coverage and allow more adsorbate adsorbate interactions, but the kinetics will of course not be the same as at high pressures at temperatures of 300 K or higher.

Chemisorption on metal oxides is quite different from that on metals. Stoichiometric metal oxide surfaces are quite unreactive compared to metal surfaces and chemisorption often takes place at defects. Defects in oxides are treated in more detail in the introduction to metal oxides in Chapter 3. According to Henrich and Cox, who in 1994 published a seminal book with the title *The Surface Science on Metal Oxides*, chemisorption on oxides can generally be categorized into three groups [10]:

(i) *Acid/base or donor/acceptor − type reactions* involve exchange of electron pairs. In chemistry, a Lewis acid is a species that accepts an electron pair while a Lewis base donates an electron pair. A metal cation is thus a Lewis acid site that preferably accepts electrons from Lewis base molecules such as H_2O or NH_3. Furthermore, oxygen anions are Lewis base sites that donate electrons to Lewis acid molecules. Acids and bases are classified in three groups; hard, intermediate and soft acids/bases. Hard acids/bases have valence electrons that are not that easily removed or polarized, while the valence electrons of soft acids/bases are easily distorted or removed. The combinations hard acid-hard base and soft-acid-soft base are more likely to occur than the combinations hard acid-soft base and soft acid-hard base. This Lewis-base concept is very useful in understanding the ion-pairing stage in the atmospheric corrosion process that is quickly summarized in the introduction of this thesis.

(ii) *Oxidation/reduction with electron transfer* occurs when there is a direct transfer of electrons to or from the surface leading to a change of oxidation state of the adsorbate. An example of this is when atomic hydrogen H reacts with a surface and forms H^+.

(iii) *Oxidation/reduction with oxygen transfer* involves transfer of an oxygen anion to or from the surface also giving a change in oxidation state of the molecule. An example of this is the reduction of an oxide surface by CO oxidation:

$$CO_{ads} + O^{2-}_{lattice} \rightarrow CO_{2,gas} + 2e^- \tag{4.1}$$

At a first glance, the difference between acid/base and oxidation/reduction reactions might seem unclear but the clear distinction is that in oxidation/reduction reactions, the number of free electronic charges of the surface is changed why it remains intact in acid/base reactions.

4.1 H_2O adsorption

Water is of paramount importance in a wide range of fields including surface chemistry. At atmospheric conditions, all surfaces are covered with a thin water layer, whose thickness depends on humidity [1]. This layer has large impact on the interaction of surfaces with the ambient atmosphere.

The geometrical structure of the isolated water molecule is characterized by an OH bond length of 0.96 Å and an H-O-H angle of 104.5° [68]. The water molecule is a good donor due to its large dipole moment and its lone-pair electrons. The interaction between water and an oxide surface is an acid/base type of reaction [10] where the water molecule interacts with acid sites of the oxide surface (metals cations). Water adsorption can be both molecular and dissociative. Dissociation involves formation of hydroxyl groups through the following reaction:

$$H_2O + O^{2-}_{lattice} \rightarrow 2OH^- \tag{4.2}$$

Dissociation is often favored on defect sites of the oxide. This explains why most polycrystalline oxide surfaces are covered with hydroxyl groups. However, many studies also propose water dissociation at non-defective oxide surfaces. Water dissociation on metal oxides is predominantly reversible, i.e. water is formed when heating the dissociation products and the desorption product is thus molecular water [69]. Moreover, water dissociation require strong bonding between the oxygen atom in the water molecule and a cation site of the oxide surface and a relatively short distance between the water molecule and an oxygen anion in the surface enabling hydrogen bonding to the surface [69]. This explains why defect sites often favors water dissociation, since defects often involve e.g. coordinatively unsaturated cation sites that is usually more acidic than the original site and thus gives a stronger bonding to the oxygen atom in the molecule. The larger number of possible coordinations on a defective surface also facilitates a short enough distance between surface cations and anions that is needed for water dissociation. More detailed information on the characteristics of the water molecule and water adsorption is found in the reviews by Henderson [69] and Thiel and Madey [70].

In this thesis, water adsorption is studied by means of STM and core level photoemission. In photoemission measurements, molecular water and hydroxyl groups can mostly be differentiated by using the shift of the water related O 1s peak to the main O 1s peak, which is assigned to oxygen in the oxide. In table 4.1, O 1s binding energies for molecular water and/or hydroxyl groups on single crystalline metal oxide surfaces are shown. The identity of the adsorbate has been confirmed with at least one additional experimental technique in all these studies. As seen in table 4.1, dissociative and molecular adsorption gives an O 1s component that is shifted with 0.6-2.1 eV respective 2.0-3.2 eV relative to the main O 1s peak.

Table 4.1. Binding energies (E_{Bin}) for O 1*s* components in PES studies of water exposed single crystal metal oxide surfaces

Oxide surface	E_{Bin} (eV) O	OH	H_2O	ΔE_{Bin} (eV) O-OH	O-H_2O	T (K)	Ref
$Al_2O_3(100)$	531.5	-	~533.5	-	~2.0	100	[71]
α-$Cr_2O_3(0001)$	531.5	532.4	534.0	0.9	2.5	250	[72]
α-$Cr_2O_3(0001)$	530.8	531.4	-	0.6	-	300	[73]
$Fe_3O_4(111)$	530.0	532.1	-	2.1	-	180	[74]
$TiO_2(110)$	530.6	532.2	-	1.6	-	300	[75]
$TiO_2(110)$	530.2	-	532.9	-	2.7	100	[76]
$V_2O_3(11\bar{1})$	530.0	531.3	533.2	1.3	3.2	180-600	[77]
$ZnO(000\bar{1})$	531.6	533.7	-	2.1	-	100	[78]

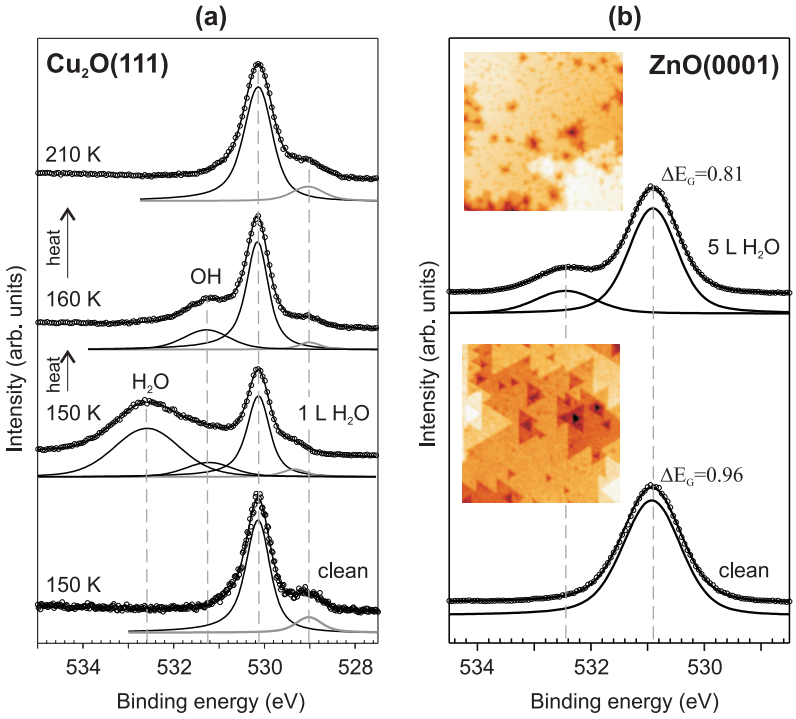

Figure 4.2. O 1*s* core level spectra from clean and H_2O exposed $Cu_2O(111)$ (a) and ZnO(0001) (b). Photon energies are 670 eV for (a) and 619 eV for (b). All water adsorption is performed at 100 K and the temperature reached after heating is given for every spectrum in the figure.

4.1.1 H_2O adsorption: Results and discussion

Water adsorption on ZnO(0001) and $Cu_2O(111)$ has been studied and O $1s$ core level spectra from these studies are shown in Figure 4.2. No water adsorbs on $Cu_2O(111)$ at room temperature. At 150 K, water dissociates partly and both molecular water and hydroxyl groups coexist on the surface, as shown in Figure 4.2 (a). The molecularly adsorbed water desorbs when heating the sample to 160 K and at 210 K, hydroxyl groups have desorbed as well. The desorption of hydroxyl groups is accompanied with an increased size of the O $1s$ peak associated with multiply undercoordinated oxygen anions. Some of the hydrogen species formed in the dissociation of water are thus adsorbed on O_{MCUS} sites. However, as earlier described, both metal cations and nearby anions are needed on the oxide surface for dissociation to appear. If the $Cu_2O(111)$-Cu_{CUS} surface model suggested by Soon et al. [12, 40] is valid, there is only one type of regular surface site, i.e. the coordinatively saturated copper ion. However, STM images of the clean surface have shown that the density of oxygen vacancies can be quite large also on surfaces which show a (1x1) LEED pattern. The most probable scenario is therefore that water adsorbs on an oxygen vacancy that is in close proximity to a copper vacancy. These adsorption sites do not seem to be favorable for OH groups though, since desorption appears already at 160 K.

The ZnO(0001) surface is shown to be more reactive to water. PES data, in Figure 4.2(b) show that water dissociates at the surface at room temperature. STM measurements show that water adsorbs along step edges, since when increasing the water dose, the terraces grow in size and pits diminish. The step edges grow in an irregular fashion, which leads to a transition from triangularly shaped islands and pits to more irregular shapes. In Figure 4.2 (b), insets of STM images of a clean and a water exposed surface are shown. In the image from a surface exposed to 5 L water, only a few triangles can be seen and at a dose of 20 L (not shown), it is hard to discern any triangular shapes at all.

Two possible reasons (or a combination of them) could be found by the author for why ZnO(0001) is more reactive to water than $Cu_2O(111)$. First, the step edges on ZnO(0001) might give a more optimum distance between cations and anions on the surface than the oxygen vacancy - copper vacancy pair on the $Cu_2O(111)$ surface. Secondly, the fact that water is classified as a hard base, while the Cu^+ ion is believed to be a soft acid might make a combination of them unfavorable [1]. Zn^{2+} ions are on the other hand classified as intermediate acids [1] and should be more probable to pair up with water.

4.2 SO_2 adsorption

Sulfur dioxide (SO_2) is an atmospheric pollutant that is created in the combustion of fuels derived from coal and oil, which mostly contain a small amount of sulfur containing impurities. It is well known that SO_2 has large impact on the corrosion of metals, but the exact reaction mechanisms are not fully understood [1]. Sulfur

dioxide is also known to cause sulfur poisoning of various catalysts [79, 80]. Such poisoning can appear when a catalyst not only catalyzes the main reaction they are used for but also the unwanted dissociation of SO_2 to sulfur. The sulfur atoms then adsorb on and block the active sites of the catalyst surface. Contrary to this, other applications demand materials that are reactive towards SO_2. To reduce the emission of sulfur oxides from various industries, much effort has been made to develop techniques for removal of SO_2 from waste gases. These techniques can be divided into two groups, i.e. wet and dry processes. In one type of dry process, the waste gas is passed over an SO_2 sorbent, typically an oxide such as CaO, Fe_2O_3, MgO or ZnO [81, 82].

The geometrical structure of the gas phase SO_2 molecule is characterized by an intramolecular S-O bond length of 1.43 Å [83] and an O-S-O angle of 119° [84]. The molecular orbitals that are mostly involved in bonding of SO_2 to a surface or another molecule are the HOMO, which has σ symmetry and LUMO, which has π symmetry [85]. Since HOMO and LUMO are mainly localized on the sulfur atom of the molecule [86], bonding of the SO_2 molecule usually appears via the sulfur atom. Bonding of SO_2 in transition metal complexes is mostly characterized by σ donation from the HOMO of SO_2 to the bonding partners and π back-donation into the LUMO of SO_2.

The SO_2 molecule has a rich coordination chemistry demonstrated by its large number of possible coordination geometries in transition metal complexes [87]. On oxide surfaces, SO_2 can adsorb molecularly by bonding of either the S atom or and O atom to a surface cation [10]. When SO_2 binds to an oxygen anion, a sulfite-like (SO_3^{2-}) species is formed giving the reaction

$$SO_2 + O^{2-}_{lattice} \rightarrow SO_3^{2-} \tag{4.3}$$

where SO_2 acts as an acceptor. However, the exact charge of the sulfite ion is usually not known and therefore it is often referred to as SO_3 [88, 89, 89, 90] but denoting them SO_3^{2-} is also quite common. There are theoretical studies on SO_2 adsorption on Ag(111) that imply that SO_3^{2-} loses most of its ionic electrons to the bulk and the SO_3 specie is then charge neutral [91]. Although the latter example is from a metallic surface with very different properties than an oxide surface, this shows that sample surface properties can largely influence the ionic charge of SO_x species. Formation of sulfate (SO_4^{2-}) can appear through interaction with two oxygen anions in the surface, giving the reaction

$$SO_2 + 2O^{2-}_{lattice} \rightarrow SO_4^{2-} + 2e^- \tag{4.4}$$

Also for sulfate-like species, the exact ionic charge is mostly not known and they are therefore often referred to as SO_4. Studies of various polycrystalline oxide surfaces [90] have shown that SO_4 formation is more common on oxygen rich oxides, e.g. TiO_2 and Cr_2O_3 while SO_3 predominates on oxides with lower oxygen content such as CuO and ZnO. A transformation from SO_3 to SO_4 species have been observed, e.g. on MgO surfaces. This transformation can be induced by heating to elevated

temperatures, by reaction with hydroxyl or water groups, by reaction with excess oxygen atoms or by exposure to intense radiation [90].

SO_2 dissociation to oxygen and atomic sulfur (S) or sulfide (S^{2-}) occurs through charge transfer to the LUMO of SO_2 and subsequent S-O bond-breaking. On all investigated metals, except for Ag and Au, SO_2 dissociates either directly upon adsorption or by subsequent heating. When coming to oxide surfaces, SO_2 decomposition is more unusual due to low charge density and if it occurs, it always takes place at metal cations. In order to increase the ability of an oxide surface to dissociate SO_2, the charge density on surface cations should be increased by creating occupied metal states above the valence band of the oxide [90]. This can be done, e.g. by creating oxygen vacancies, doping with transition metal ions or addition of alkali metals in the oxide structure [90].

In the work presented in this thesis, photoelectron spectroscopy has been the most useful tool for identifying reaction products upon SO_2 reaction products. The S $2p$ binding energy increases with the oxidation number of sulfur and S, SO_2, SO_3 and SO_4 species are quite readily identified. S $2p$ binding energies for SO_2 exposed single crystalline samples are listed in table 4.2. From this table and some data not shown in the table [92–94] it is shown that sulfur or sulfide species typically has an S $2p$ binding energy of ∼160-162 eV and that the shifts for SO_3 and SO_4 related peaks from the sulfur/sulfide peak are 4.2-4.9 eV and 5.0-7 eV respectively.

4.2.1 SO_2 adsorption: Results and discussion

Adsorption of sulfur dioxide on ZnO(0001) and Cu_2O(111) has been studied and PES data from these studies are shown in Figure 4.3. When Cu_2O(111) is exposed to SO_2 at a dosing pressure of $4{\cdot}10^{-9}$ mbar, the size of the S $2p$ peak remains constant above an SO_2 dose of 1.5 L and the surface is thus saturated with SO_2, at least at the low pressure used when dosing. The S $2p$ peak is positioned at a binding energy of 166.3 eV as seen in the bottom spectrum in Figure 4.3 a. It is shifted from the small atomic sulfur peak at 161.5 eV with 4.8 eV, which is typical for SO_3 species. A small component at 168 eV improves the fit and it can be assigned to SO_4 species. The O $1s$ spectrum from the SO_2 saturated Cu_2O(111) surface shows an SO_x related component at 530.8 eV, shifted from the main O $1s$ peak with 0.8 eV. The small relative size of this component indicates that SO_3 formation occur at defects only. Since SO_2 adsorption is accompanied with a decrease of the relative size of the O_{MCUS} related O$1s$ peak, SO_2 appears to adsorb at O_{MCUS} anions to form SO_3. Other defects might act as adsorption sites as well.

S $2p$ spectra from a ZnO(0001) surface exposed to 0.5 L and 5 L SO_2 are shown in Figure 4.3 a. The main component at 167.4-167.6 eV is shifted from the atomic sulfur peak at 162.1-162.4 eV with 5.0-5.5 eV. In a study by Rodriguez et al.[102], SO_2 adsorption at room temperature on ZnO(0001) gave an S $2p$ peak at ∼166.5 eV and a shift from the small atomic sulfur peak (only observed on the sputtered surface) of ∼4.8 eV. They assigned this peak to SO_3 species, which was confirmed by NEXAFS measurements. This indicates that the S $2p$ peaks in Figure 4.3 a can

Table 4.2. Binding energies (E_{Bin}) and binding energy shifts (ΔE_{Bin})(ΔE_{Bin} is the shift for an SO_x component to the S component) for S $2p_{3/2}$ lines measured with photoelectron spectroscopy for different SO_2 adsorption products on single crystal metal and metal oxide surfaces

Sample surface	E_{Bin} (eV)				ΔE_{Bin} (eV) (E_{Bin} - $E_{Bin,S}$)			T (K)
	S	SO_2	SO_3	SO_4	SO_2	SO_3	SO_4	
Ag(110)[95]	-	165.4	166.1	167.9	-	-	-	300
Ag(111)[96]	-	-	165.5	167.3	-	-	-	230-700
Cu(111)[97]	160.2	164.1	-	-	-	-	-	170-450
Ni(111)[98]	162.0	-	166.7	-	-	4.7	-	300
Ni(100)[96]	161.3	-	165.9	-	-	4.6	-	300
CeO_2(111)[88]	-	-	166.9	168.2	-	-	-	150
Cr_2O_3(0001)[89]	161.9	164.5	166.3	168.2	2.6	4.4	6.3	100-450
Fe_3O_4(100)[99]	161.3	-	166.2	167.1	-	4.9	5.8	300
MgO(100)[100]	-	-	166.3	168.4	-	-	-	300
TiO_2(110)[101]	162	-	-	167.5	-	-	5.5	300-600
ZnO(0001)[102]	161.7	165.0	166.5	-	3.4	4.8	-	100-600
ZnO($000\bar{1}$)[103]	-	-	166.4	-	-	-	-	110-150
ZnO poly[104]	-	165.8	166.8	168.2	-	-	-	100
compounds[105]	162.0	-	166.7	169	-	4.7	7	300

be attributed to SO_3. However, when comparing to typical binding energies and shifts on other oxide and metal surfaces, it is not evident whether we have SO_3 or SO_4 species on the surface and therefore we hereafter call them SO_x species. The spectra are quite wide and can be divided into two components at ∼167.2 and ∼167.8 eV respectively. However, the components are not resolved and the spectra could as well be divided into three or more components. The small shift between the two fitted components indicates that they should not be associated to SO_3 and SO_4 species respectively but rather to two types of either SO_3 or SO_4 species.

It should be noted that the SO_2 adsorption studies on ZnO(0001) that are presented in Figure 4.3 involve a sample that during the cleaning cycle has been annealed to only 530°C. We have observed that a higher annealing temperature (∼ 600°C) gives a more well-ordered surface. The reason for using a sample annealed at 530°C was that when annealing to 600°C and then adsorbing SO_2, the sample charging became so severe that measurement was not anymore possible. However, when measuring on the clean surface, no sample charging was observed. It thus seems as if SO_2 adsorption lowers the conductivity of the well-ordered ZnO(0001) surface. A change in conductivity upon adsorption of molecules is a phenomenon that is used in gas sensing and ZnO is also a potential material for gas

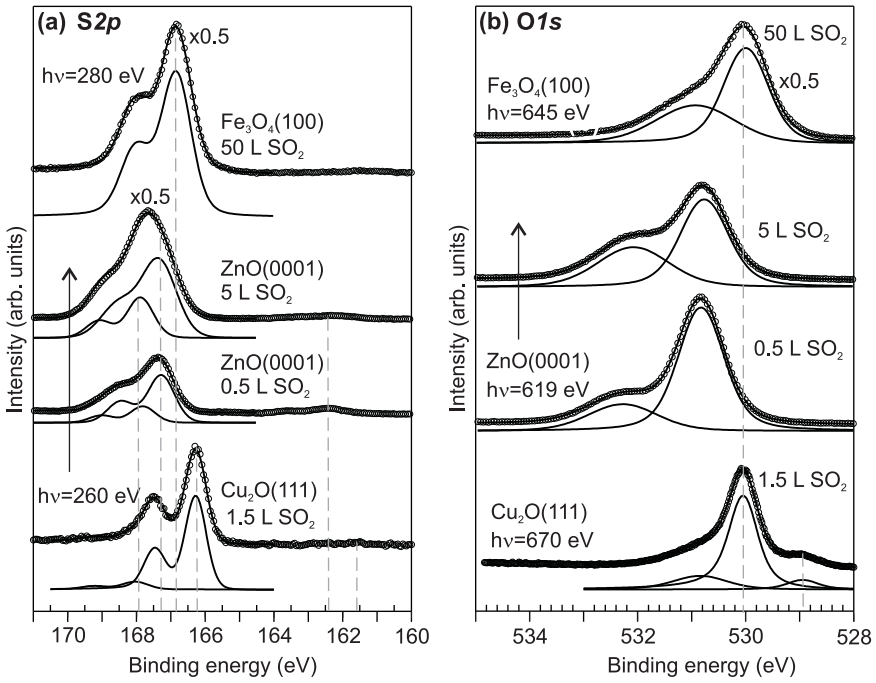

Figure 4.3. S 2p (a) and O 1s (b) core level spectra from SO_2 exposed $Cu_2O(111)$, ZnO(0001) and $Fe_3O_4(100)$. Adsorption and measurement are performed at room temperature.

sensing applications. In contrast to our study on ZnO(0001), SO_2 adsorption on polycrystalline ZnO has earlier been observed to give an increase in conductivity. However, polycrystalline ZnO contains various surfaces where (0001) is only one of them and there is a large variation in gas sensing properties for different surfaces. Then one arrives to the question why the sample charging problems only appeared on the higher annealed sample. First, the reason for this could be that annealing at 600°C gives a lower conductivity of the sample due to that hydrogen dopants have been annealed out from the crystal as discussed in section 3.2.1.

The second explanation for why surface conductivity after SO_2 adsorption is lower on the well-ordered surface is based on equations 4.3 and 4.4 or modifications of them. These reaction formulas show that sulfate formation involves a transfer of free electrons to the surface, while sulfite formation gives no such surface reduction. Even though oxygen anions mostly are assumed to have a charge of -2, this is not always the case in metal oxides [10]. If equation 4.3 is modified, by replacing the $O^{2-}_{lattice}$ ion with $O^{-}_{lattice}$, sulfite formation will lead to a charge transfer away from the surface, which will lead to a decrease of the surface conductivity as observed.

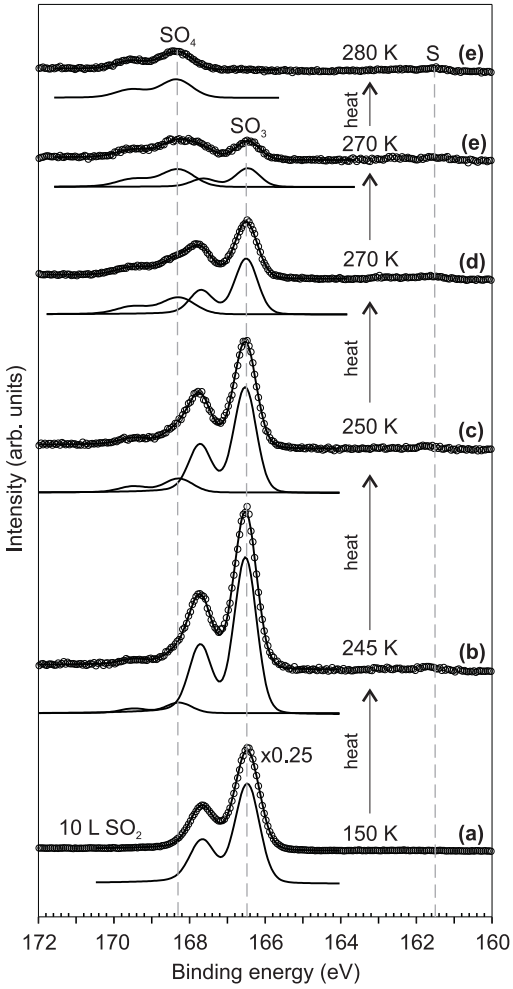

Figure 4.4. S 2*p* core level spectra ($h\nu$=260 eV) from SO_2 exposed $Cu_2O(111)$. Adsorption is performed at 150 K and then the sample temperature has been increased slowly.

If SO_2 interaction with the well-ordered surface gives sulfite groups while sulfate is formed on surfaces with a lower degree of order, this would then explain a larger electron density in the latter case.

On $Fe_3O_4(100)$, SO_2 interacts with two oxygen sites giving SO_4 species, whose adsorption pattern appears to follow the $(\sqrt{2} \times \sqrt{2})R45^\circ$ reconstruction.

The difference in SO_2 reactivity between the different samples is not that large as when comparing water reactivity of $Cu_2O(111)$ and $ZnO(0001)$ at room temperature. SO_x species form on all surfaces and depending on the actual surface structure and the order on the surface x=3 or x=4. As already known, SO_4 formation demands a quite short distance between O sites in the surface. However, SO_4 could also form by the interaction of e.g. two SO_3 species but this demands a close contact between the two species, which is not likely at the low SO_x coverages that is often obtained when SO_2 adsorb on defects only. Higher coverages can be obtained in UHV-based measurements by lowering the temperature. In Figure 4.4, S $2p$ spectra from low temperature adsorption of SO_2 on $Cu_2O(111)$ are shown. At 150 K, SO_2 interacts with the surface to give SO_3 species. The saturation coverage is much higher than at room temperature although no multilayers are formed. When heating the SO_3 covered surface a new S $2p$ component assigned to SO_4 species appears and grows stronger in the same time as the SO_3 diminish in size. At 280 K, only SO_4 species remains on the surface. We believe that the SO_4 formation is due to interaction between two different SO_3 species, where one of them is only present on the surface at lower temperatures than room temperature. The two types of SO_3 species are associated with two different adsorption sites.

4.3 H_2O and SO_2 coadsorption

At atmospheric conditions, SO_2 interacts with the water layer covering all surfaces by the following reactions [106]:

$$SO_2 + xH_2O \rightleftharpoons SO_2 \cdot xH_2O \tag{4.5}$$

$$SO_2 \cdot xH_2O \rightleftharpoons HSO_3^- + H_3O^+ + (x\text{-}2)H_2O \tag{4.6}$$

$$HSO_3^- \rightleftharpoons H^+ + SO_3^{2-} \tag{4.7}$$

Further oxidation of sulfite or bisulfite ions can appear through the reaction with peroxide [106]:

$$HSO_3^- \xrightarrow{H_2O_2} SO_4^{2-} \tag{4.8}$$

or slowly through the reaction with oxygen [106]:

$$SO_2 + xH_2O + \frac{1}{2} \cdot O_2 \rightarrow H_2SO_4 \tag{4.9}$$

Formation of sulfate ions or sulfuric acid can also be promoted by ozone, an increased pH and by catalysts containing Fe^{3+} and Mn^{2+} ions [106]. A large number

of studies have been made on the interaction of SO_2 with an oxidized metal surface covered with a thin water layer. Still, this system is not yet thoroughly described at a molecular level. Since water is always present at surfaces at atmospheric conditions, it is very important to introduce water in order to understand e.g. corrosion or catalysis related SO_2 surface reactions.

Only a few well-controlled surface science studies on the coadsorption of water and SO_2 have been found by the author. Water was shown to have minor effects on the SO_2 chemistry on oxidized or reduced $CeO_2(111)$ films on Ru(0001) [107]. On MgO(100), water or hydroxyl groups have been shown to induce an SO_3 to SO_4 transformation [100]. Hydroxylation has been shown to reduce the SO_2 reactivity of Cu(110) [108]. Moreover bisulfates (HSO_4^-) were observed on the prehydroxylated Cu(110) surface. H_xSO_4 species or SO_4 ions solvated by chemisorbed water have also been observed upon SO_2 adsorption on an ice multilayer on Zn(0001) at 100 K [109]. Sulfate-like species were stable well above 300 K when heating this SO_2 exposed ice layer. When exposing the clean Zn(0001) surface to SO_2, however, SO_3 species were formed. Similar to the case of MgO(100), water on Zn(0001) thus appears to favor SO_4 groups at the expense of SO_3.

4.3.1 H_2O and SO_2 coadsorption: Results and discussion

Water and SO_2 coadsorption studies have been performed on ZnO(0001) (a) and $Fe_3O_4(100)$ (b) samples. Here, the term coadsorption does not denote the simultaneous adsorption of two species, but two subsequent dosings. In Figure 4.5, S $2p$ spectra from SO_2 exposed surfaces are compared to spectra from surfaces exposed to water and then a dose of SO_2. For ZnO(0001) (see Figure 4.5 a), water have two main effects on SO_2 chemistry. First, less SO_x groups are formed, which is probably due to that hydrogen created in the dissociation of water on ZnO(0001) occupies SO_2 adsorption sites. Secondly, more atomic sulfur is shown to form on the prehydroxylated surface. The second effect has only been observed on samples annealed at 530°C in the sample preparation procedure (sample B). Water has not shown this effect on samples annealed at 450°C (sample A). We suggest that oxygen vacancies combined with hydrogen could act as n-type donors and cause downward band bending at the surface. The higher charge density at the surface would then enable a charge transfer to the SO_2 molecule, which is needed for SO_2 dissociation. A larger number and perhaps also different types of oxygen vacancies could be created at the higher annealing temperature of 530°C. This could explain why no atomic sulfur is observed on prehydroxylated sample A surfaces.

Water and SO_2 coadsorption on $Fe_3O_4(100)$ has been studied by means of PES. The two measurements on SO_2 adsorption and coadsorption with water shown in Figure 4.5(b) are performed at different measurement occasions. It is thus questionable as to whether one should draw definitive conclusions on the effect of water from this data. What can be observed from the spectra obtained is that there are two main differences between the SO_2 chemistry on the clean and water exposed surfaces studied. First a large amount of SO_3 is formed on the water exposed

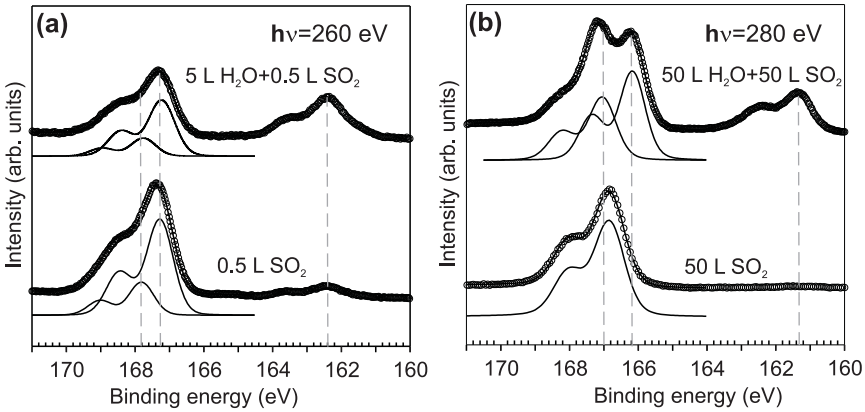

Figure 4.5. S $2p$ core level spectra from SO_2 adsorbed on clean or water exposed ZnO(0001) (a) and Fe_3O_4(100) (b).

surface but none on the clean surface. This is quite unexpected, since water has shown to favor SO_4 groups at the expense of SO_3. The second effect of water is that a larger amount of atomic sulfur is formed on the water pre-exposed surface. This effect is similar to what was observed on ZnO(0001) sample B surfaces. It indicates that water adsorption gives a higher charge density at the surface, which has not been reported in the literature. However, saturation coverage of hydrogen species has shown to induce a semiconductor-half metal transition of the surface. The role of water in the SO_2 chemistry on this surface is yet unclear and more measurements are needed to investigate this further. LEED and STM show that the SO_x adsorbates follows the $(\sqrt{2} \times \sqrt{2})$R45° reconstruction of the clean surface.

The water-SO_2 coadsorption studies we have made are just starting points and more studies are needed to understand complicated situation with two adsorbates and a defective oxide surface. What we can conclude from these results is that the interaction between these two molecules is not as expected from experiments performed at atmospheric pressure. Most likely, the unexpected results from the UHV-based studies are not only due to the pressure gap but also due to the material gap. While corrosion studies are typically performed on polycrystalline samples, studies performed at UHV conditions are done on single crystalline samples. Another important factor is that the sputtering and annealing procedures used to clean single crystalline samples often leads to oxygen deficient crystals and defects related to oxygen deficiency can have vast effects on the properties of an oxide crystal. Metal oxide based catalysts can e.g. be intentionally reduced e.g. by reaction with hydrogen gas in order to improve catalyst reactivity. The effects of water on SO_2 chemistry on ZnO(0001) and Fe_3O_4(100) could thus be more relevant for catalytic applications than for understanding corrosion mechanisms.

Chapter 5

Summary of papers

5.1 Paper 1 - Probing the valence band structure of Cu_2O using high-energy angle-resolved photoemission

The valence band structure of Cu_2O along the Γ-M direction is studied by means of ARPES at T=100 K. The only other published ARPES study of Cu_2O prior to this paper is performed along the Γ-R direction using low photon energies. Due to the use of high photon energies ($h\nu$=619 eV and 891 eV) and an effective background subtraction, our data gives a clearer picture of the bulk band structure than the previous study. Moreover, these data give the first experimental evidence of a hybridized Cu $3d$-Cu $4s$ state located between the two main Cu $3d$ and O $2p$ band regions. The measured band structure is compared to theoretical local density approximation (LDA) band structure calculations with and without the Hubbard U potential. An adjustement of the U value in the (LDA+U) calculations gives good agreement with measured data.

Contributions of the candidate: I have been part of the data acquisition, data analysis and the submission process for this paper. I have also been responsible for preparing a first version of the paper.

5.2 Paper 2 - Atomic structure of $Cu_2O(111)$

The clean $Cu_2O(111)$ surface structure is investigated with LEED and STM. Annealing in oxygen is shown to give a stoichiometric (1×1) oxygen terminated surface while annealing in ultra-high vacuum results in a $(\sqrt{3} \times \sqrt{3})$R30° reconstruction and surface faceting. The reconstruction is interpreted as one-third of ordered oxygen vacancies as suggested in an earlier study. A detailed STM image of a surface with both (1x1)-terminated and reconstructed regions is compared to two surface models, one bulk-terminated surface and one where undercoordinated copper ions are missing. However, no definite conclusions on the exact surface structure can be drawn from the data.

Contributions of the candidate: I have had a central part in the planning of experiments, data acquisition, data analysis, submission process and writing of the first version of the paper.

5.3 Paper 3 - Role of defects in surface chemistry on $Cu_2O(111)$

STM and high resolution PES is used to study $Cu_2O(111)$ and its interaction with water and SO_2. It is shown by STM that oxygen vacancies can be ordered in the $(\sqrt{3} \times \sqrt{3})R30°$ reconstruction or randomly distributed on (1x1)-terminated surfaces. The number of oxygen vacancies depends on sample preparation and on sample history. Multiply undercoordinated oxygen anions (O_{MCUS}) such as oxygen anions adjacent to copper vacancies are believed to be adsorption sites for both hydrogen from dissociated water and for SO_2. Water adsorption at 150 K gives a small amount of hydroxyl groups but the major part of the water adsorbs molecularly. The molecular water desorbs at 160 K and at 200 K, the OH groups desorb as well. At room temperature, SO_2 adsorbs at defect sites such as O_{MCUS} sites and SO_3 species are formed. SO_3 species are also formed upon adsorption at 150 K and the coverage is much higher than at room temperature. When heating this SO_3 layer, SO_2 desorbs and SO_3 species are replaced with a small amount of SO_4 species and at 280 K, only SO_4 remains on the surface. SO_4 formation is believed to occur through interaction between SO_3 groups on the surface enabled by the higher coverage at lower temperatures.

Contribution of the candidate: I have had a central part in the planning of experiments, data acquisition, data analysis, submission process and writing of the first version of the manuscript.

5.4 Paper 4 - Water Adsorption on ZnO(0001): Transition from Triangular Surface Structures to a Disordered Hydroxyl Terminated Phase

Water adsorption on the zinc-terminated ZnO(0001) surface at room temperature is studied with STM and PES. The water adsorption is shown to be dissociative and appears at step edges. Water dissociation is believed to occur through bonding between oxygen in the molecule and surface cations close to step edges and bonding of hydrogen in the molecule with the undercoordinated oxygens at step edges. The clean ZnO(0001) surface is covered with triangular structures. When the water dose is increased, step edges become more and more irregular, terraces grow and pits diminish. At a water dose of 20 L, the surface structure is very irregular and hydrogen created in the dissociation reaction of water is believed to be responsible for this.

Contributions of the candidate: I have had a central part in the planning of experiments, data acquisition, data analysis, submission process and writing of the first version of the paper.

5.5 Paper 5 - SO_2 Interaction with Zn(0001) and ZnO(0001) and the Influence of Water

Water and SO_2 interaction with Zn(0001) and ZnO(0001) surfaces at room temperature is studied by means of PES. No water adsorb on Zn(0001), while hydroxyl groups are formed on ZnO(0001), which confirms earlier observations that oxygen is important in the water-zinc interaction. The reaction between SO_2 and Zn(0001) is aggressive giving a complete oxidation of the surface and formation of various sulfur containing species. Complete dissociation of SO_2 is shown to be more efficient than on polycrystalline zinc. SO_2 adsorption on ZnO(0001) gives mostly SO_3/SO_4 species. The sample preparation and especially the annealing temperature of ZnO(0001) can have large effects on chemical properties of this surface. The oxygen deficiency of the crystal increases with annealing temperature. In addition, at certain temperatures different types of hydrogens are annealed out from the crystal. Since hydrogen can act as shallow donors, it can highly influence surface properties. Water is shown to have different effect on SO_2 chemistry on samples that have been annealed at 450°C and 530°C in the preparation procedure. On the former sample, water just block SO_2 adsorption sites, while it has an additional and surprising effect on the latter sample, namely an increased degree of SO_2 dissociation. This effect is unexpected, since it indicates that water increases the charge density on the ZnO(0001) surface and water is generally believed to have the opposite effect. We suggest that a combination of hydrogen species and oxygen vacancies could give n-type surface donors that could explain this effect.

Contributions of the candidate: I have had a central part in the planning of experiments, data acquisition, data analysis, submission process and writing of the first version of the manuscript.

5.6 Paper 6 - High resolution spectroscopic and microscopic signatures of ordered growth of ferrous sulfate in SO_2 assisted corrosion of Fe_3O_4(100)

STM and PES studies of a Fe_3O_4(100) surface exposed to 50 L water followed by 50 L SO_2 have been made. PES reveal the formation of SO_3 as well as SO_4 and S species. The SO_x species are shown to be locked in the $(\sqrt{2} \times \sqrt{2})$R45° surface potential. In this paper it is stated that 'Positive bias means tunneling from occupied states', where positive should be replaced by negative. Moreover, 1 L is given as (1 L = 10^{-6} mbar s), where mbar should be replaced by torr.

Contributions of the candidate: I have participated in the PES measurements and in discussing the obtained results.

Chapter 6

Now this is not the end. It is not even the beginning of the end, but it is, perhaps, the end of the beginning.

Winston Churchill (1874 - 1965)

Conclusions and future outlook

This thesis present studies on metal oxide surfaces and their interaction with water and sulfur dioxide. When studying molecular interaction with an oxide surface, it is very useful to first have a clear picture of the structure of the clean surface. It is also important to discern the impact of the sample preparation on surface stoichiometry and structure. We have studied surface structure and composition of $Cu_2O(111)$ and ZnO(0001). In the studies of $Cu_2O(111)$, two point defects are identified, i.e. oxygen vacancies and copper vacancies. When annealing in UHV, a $(\sqrt{3} \times \sqrt{3})R30°$ reconstruction, based on oxygen vacancies is obtained. The copper vacancies are shown to be reactive towards both water and SO_2. In the study of ZnO(0001), sample annealing temperature (in the sample preparation procedure) is shown to have significant impact on surface composition and reactivity. Oxygen vacancies and hydrogen dopants are believed to play important roles in the variation of properties of the differently prepared surfaces. The work with these surfaces has raised new questions and here follows a few important and interesting points, which deserve further studies:

- The exact atomic structure of $Cu_2O(111)$ and experimental evidence on whether the $Cu_2O(111)$-Cu_{CUS} surface model is valid or not
- Surface electronic structure of (1x1) and $(\sqrt{3}\times\sqrt{3})R30°$-terminated $Cu_2O(111)$
- How the electronic structure of bulk ZnO and the ZnO(0001) surface evolves when increasing the annealing temperature
- Hydrogen content in bulk ZnO and in the ZnO(0001) surface as a function of annealing temperature

The initial intention of this thesis was to get a better understanding at a molecular level of the aqueous layer and of SO_2-induced atmospheric corrosion on metal oxide surfaces. We have approached the problem by performing adsorption and coadsorption studies with water and sulfur dioxide on $Cu_2O(111)$, ZnO(0001) and $Fe_3O_4(100)$. Water adsorption is shown to be dissociative on ZnO(0001) and partly

dissociative on $Cu_2O(111)$. Defects are involved in the dissociation process on both surfaces. Water adsorbs on ZnO(0001) at room temperature but $Cu_2O(111)$ is less reactive to water and all water has desorbed from this surface at 210 K. SO_2 adsorbs on defect O-sites on both ZnO(0001) and $Cu_2O(111)$ but on $Fe_3O_4(100)$, the adsorption pattern appears to follow the $(\sqrt{2} \times \sqrt{2})R45^\circ$ reconstruction. When SO_2 adsorbs on an oxygen site, SO_3 forms. SO_4 formation requires two rather closely situated oxygen sites or interaction between two SO_3 species. The latter process has been observed upon low temperature ($\sim$150 K) adsorption of SO_2 on $Cu_2O(111)$ and subsequent heating.

While the outcomes from the water and SO_2 adsorption studies are reasonable and quite expected, the coadsorption studies give more surprising results. The most unexpected effect of water is that it appears to increase the charge density at the surface on both $Fe_3O_4(100)$ and on one type of ZnO(0001) sample. This is shown through a higher degree of dissociation of SO_2 to atomic sulfur or sulfide on the water exposed surface. In the case of ZnO(0001), we suggest that oxygen vacancies in combination with hydrogen created in the water dissociation reaction could serve as n-type donors that could explain the increased conductivity. For $Fe_3O_4(100)$, no mechanism of the effect of water has been suggested and more studies are needed on water and SO_2 coadsorption on both oxide surfaces for a detailed picture of the surface reactions.

Then one arrives to the question whether these coadsorption studies are relevant for understanding SO_2-induced corrosion of oxides. Surfaces obtained upon sputtering and annealing a single crystalline sample in UHV can be quite far from the polycrystalline metal oxide layers formed at atmospheric conditions on metal surfaces. Moreover, the kinetics and adsorbate coverages can be very different at UHV conditions than at atmospheric conditions. The differences between conventional 'Surface Science' experiments and 'real world' applications are often referred to as the *materials gap* and *pressure gap* respectively. These gaps are often mentioned within the context of model studies for catalysis. Some studies show that it is important to 'mind the gap' due to e.g. significant differences in properties between catalytic properties of nanoparticles at ambient pressures and single crystals studied in UHV [110]. Other studies show that similar adsorption structures as obtained at high pressures can be obtained at low pressures and low temperatures [111, 112]. However, it is still very important to complement UHV studies with high pressure studies in order to know if it is possible and in that case how to extrapolate UHV studies to high pressure studies [111, 112]. High pressure studies, which give information on a molecular level can be done by integrating a high pressure cell in a UHV chamber and using techniques such as high pressure sum frequency generation (SFG) vibration spectroscopy, high pressure XPS, and quartz crystal microbalance (QCM) [113].

An important factor that could make our water and SO_2 coadsorption studies differ from what we know from SO_2-induced corrosion at atmospheric conditions, is the sample preparation. Oxygen deficient samples obtained when annealing in UHV or at low oxygen pressures could have very different surface properties than more

oxygen-rich oxide layers found on metal surfaces at ambient pressures. However, oxygen deficiency can be useful in the field of catalysis, where metal oxide catalysts are sometimes deliberately reduced to improve their efficiency. This means that the unexpected effects observed in the coadsorption studies here might be more interesting for catalytic applications than for understanding corrosion.

Another significant difference between the studies presented here and 'real corrosion' is the water layer, which is often 2-10 monolayers thick at atmospheric conditions but only part of a monolayer or even nonexisting at room temperature when adsorption is made in a UHV chamber. An important step in understanding SO_2-induced corrosion is to get a better picture of *proton- and ligand-induced metal dissolution*. This is an electrochemical process that appears in liquids, although the two innermost water layers adsorbed on surfaces have shown to be rather immobile [106]. One way to approach the atmospheric corrosion conditions in a UHV chamber could be by performing studies at low temperature. Adsorption of water multilayers mixed with small amounts of SO_2 and subsequent slow heating might give a moment when this water layers become liquid-like. If continuous measurements are performed during a slow sample heating, one might be able to catch information from this liquid-like layer. If this isn't possible with the equipment available, one can study the reaction products that remain after desorption of the water multilayers. In studies of SO_2 adsorption on an ice layer on polycrystalline zinc and subsequent heating, Jirsak et al. [109] concluded that H_xSO_4 species or SO_4 ions solvated by chemisorbed water were formed. The only way to find out whether these types of adsorption experiments can give valuable information or not is to compare them to high pressure experiments. Here follows some suggestions on how to approach a better understanding at a molecular level of SO_2-induced corrosion:

- investigate effects of metal oxide sample preparation on both bulk and surface defects and stoichiometry by e.g. sputtering and annealing at different oxygen pressures
- study the structure and stoichiometry of oxide layers formed at ambient conditions and try to approach these surface conditions when preparing the sample at UHV conditions
- explore the properties and structure of a water layer going from part of a monolayer to several layers, similar to the studies by Andersson et al. on water adsorption on Cu(110) [112]
- study the interaction of SO_2 with water exposed metal oxide surfaces, where the water layer thickness ranges from part of a monolayer to multilayers

If these types of studies are done on single-crystalline surfaces and under highly controlled conditions, they will add a new dimension to the current understanding of SO_2-accelerated atmospheric corrosion.

Bibliography

[1] C. Leygraf. *Atmospheric Corrosion*. Wiley, New York, 2000.

[2] Varian Vacuum Products. *Basic Vacuum Practice*. Varian Associates, Inc., MA, US, 1992.

[3] Lüth. *Solid Surfaces, Interfaces and Thin Films*. Springer, Germany, 2001.

[4] G. A. Somorjai. *Introduction to Surface Chemistry and Catalysis*. Wiley, New York, 1994.

[5] Wikipedia, photoemission spectroscopy, February 2011. URL `http://en.wikipedia.org/wiki/Photoemission_spectroscopy`.

[6] S. Hagström, C. Nordling, and K. Siegbahn. *Physics Letters*, 9:1964, 1964.

[7] E-E. Koch. *Handbook on Synchrotron Radiation, Volume 1a*. North-Holland Publishing Company, 1983.

[8] C. Bai. *Scanning Tunneling Microscopy and its Application*. Shanghai Scientific & Technical Publishers and Springer-Verlag Berlin Heidelberg, 1995.

[9] R. M. Tromp, E. J van Loenen, J. E. Demuth, and N. D. Lang. *Phys. Rev. B*, 37:9042, 1988.

[10] V. E. Henrich and P. A. Cox. *The Surface Science of Metal Oxides*. Cambridge University Press, 1994.

[11] A. Krätschmer, I. Odnevall Wallinder, and C. Leygraf. *Corr. Sci.*, 44:425, 2002.

[12] A. Soon, M. Todorova, B. Delley, and C. Stampfl. *Surf. Sci.*, 601:5809, 2007.

[13] E. I. Solomon, P. M. Jones, and J. A. May. *Chem. Rev.*, 93:2623, 1993.

[14] V. Georgieva and M. Ristov. *Sol. Energy Mater. Sol. Cells*, 73:67, 2002.

[15] M. Hara, T. Kondo, M. Komoda, S. Ikeda, K. Shinohara, A. Tanaka, J.N. Kondo, and K. Domen. *Chem. Commun.*, page 357, 1998.

[16] S. Nikitine, J. B. Grun, and M. Sieskind. *J Phys. Chem. Solids*, 17:292, 1961.

[17] Ch. Uihlein, D. Fröhlich, and R. Kenklies. *Phys. Rev. B*, 23(6):2731, 1981.

[18] A. F. Wright and J. S. Nelson. *J. Appl. Phys.*, 92:5849, 2002.

[19] J. M. Zuo, M. Kim, M. O'Keeffe, and J. C. H. Spence. *Nature*, 401:49, 1999.

[20] S. G. Wang and W. H. Eugen Schwarz. *Angew. Chem. Int. Ed.*, 39(10):1757, 2000.

[21] S. Nagel. *J. Phys. Chem. Solids*, 46:743, 1985.

[22] P. Marksteiner, P. Blaha, and K. Schwarz. *Z. Phys. B: Condens. Matter*, 64: 119, 1986.

[23] T. Lippmann and J. R. Schneider. *J. Appl. Crystallogr.*, 33:156, 2000.

[24] E. Ruiz, S. Alvarez, P. Alemany, and R. A. Evarestov. *Phys. Rev. B*, 56(12): 7189, 1997.

[25] R. Laskowski, P. Blaha, and K. Schwarz. *Phys. Rev. B*, 67:075102, 2003.

[26] J. Ghijsen, L. H. Tjeng, H. Eskes, G. A. Sawatzky, and R. L. Johnson. *Phys. Rev. B*, 42(4):2268, 1990.

[27] K. M. Merz, Jr. and R. Hoffmann. *Inorg. Chem.*, 27:2120, 1988.

[28] F. Bruneval. *Exchange and correlation in the electronic structure of solids from silicon to cuprous oxide: GW approximation and beyond, PhD Thesis, Ecole Polytechnique, Palaiseau, France.* 2005.

[29] A. Filippetti and V. Fiorentini. *Phys. Rev. B*, 72:035128, 2005.

[30] L. E. Orgel. *J. Chem. Soc. (Resumed)*, page 4186, 1958.

[31] F. Bruneval, N. Vast, L. Reining, M. Izquierdo, F. Sirotti, and N. Barrett. *Phys. Rev. Lett.*, 97:267601, 2006.

[32] Y. Tang, Z. Chen, Z. Jia, L. Zhang, and J. Li. *Mater. Lett.*, 434:434, 2005.

[33] H. Qiu, L. Lu, X. Huang, and Y. Qu. *Electrochim. Acta*, 434:434, 2010.

[34] Z. Zhang, C. Dong, C. Yang, D. Hu, J. Long, L. Wang, H. Li, Y. Chen, and D. Kong. *Adv. Synth. Catal.*, 352:1600, 2010.

[35] F. Jensen, F. Besenbacher, and I. Stensgaard. *Surf. Sci.*, 269/270:400, 1992.

[36] F. Jensen, F. Besenbacher, E. Lægsgaard, and I. Stensgaard. *Surf. Sci. Lett.*, 259:L774, 1991.

[37] T. Matsumoto, R. A. Bennett, P. Stone, T. Yamada, K. Domen, and M. Bowker. *Surf. Sci.*, 471:225, 2001.

[38] F. Wiame, V. Maurice, and P. Marcus. *Surf. Sci.*, 601:1193, 2007.

[39] M. M. Islam, B. Diawara, V. Maurice, and P. Marcus. *J. Mol. Struct. Theochem*, 903:41, 2009.

[40] A. Soon, X-Y. Cui, B. Delley, S-H. Wei, and C. Stampfl. *Phys. Rev. B*, 79: 035205, 2009.

[41] K. H. Schulz and D. F. Cox. *Phys. Rev. B*, 43(2):1610, 1991.

[42] S. L. Harmer, W. M. Skinner, A. N. Buckley, and L-J. Fan. *Surf. Sci.*, 603: 537, 2009.

[43] M. S. Spencer. *Top. Catal.*, 8:259, 1999.

[44] Wikipedia, zinc oxide, February 2011. URL `http://en.wikipedia.org/wiki/Zinc_oxide`.

[45] A. Janotti and C. G. Van der Walle. *Rep. Prog. Phys.*, 72:126501, 2009.

[46] E. V. Monakhov, A. Y. Kuznetsov, B. G. Svensson. *J. Phys. D: Appl. Phys.*, 42:153001, 2009.

[47] E. V. Lavrov, F. Herklotz, and J. Weber. *Phys. Rev. B*, 79:165210, 2009.

[48] E. V. Lavrov, J. Weber, F. Börrnert, C. G. Van de Walle, and R. Helbig. *Phys. Rev. B*, 66:165205, 2002.

[49] G. A. Shi, M. Saboktakin, M. Stavola, and S. J. Pearton. *Appl. Phys. Lett.*, 85:5601, 2004.

[50] E. V. Lavrov, F. Herklotz, and J. Weber. *Phys. Rev. Lett.*, 102:185502, 2009.

[51] C. Wöll. *Prog. Surf. Sci.*, 82:55, 2007.

[52] O. Dulub, U. Diebold, and G. Kresse. *Phys. Rev. Lett.*, 90:016102, 2003.

[53] F. Ostendorf, S. Torbrügge, and M. Reichling. *Phys. Rev. B*, 77:041405(R), 2008.

[54] S. Torbrügge, F. Ostendorf, and M. Reichling. *J. Phys. Chem. C*, 113:4909, 2009.

[55] M. Valtiner, M. Todorova, G. Grundmeier, and J. Neugebauer. *Phys. Rev. Lett.*, 103:065502, 2009.

[56] M. J. Lyle, O. Warschkow, B. Delley, and C. Stampfl. *Phys. Rev. B*, 82: 165401, 2010.

[57] M. Valtiner, S. Borodin, and G. Grundmeier. *Phys. Chem. Chem. Phys.*, 9: 2406, 2007.

[58] G. Kresse, O. Dulub, and U. Diebold. *Phys. Rev. B*, 68:245409, 2003.

[59] M. H. Allen, C. H. Swartz, T. H. Myers, T. D. Veal, C. F. McConville, and S. M. Surbin. *Phys. Rev. B*, 81:075211, 2010.

[60] D. G. Rethwisch and J. A. Dumesic. *J. Catal.*, 101:35, 1986.

[61] E. J. W. Verwey. *Nature*, 144:327, 1939.

[62] G. Tarrach, D. Bürgler, T. Schaub, R. Wiesendanger, and H.-J. Günterodt. *Surf. Sci.*, 285:1, 1993.

[63] B. Stanka, W. Hebenstreit, U. Diebold, and S. A. Chambers. *Surf. Sci.*, 448: 49, 2000.

[64] R. Pentcheva, W. Moritz, J. Rundgren, S. Frank, D. Schrupp, and M. Scheffler. *Surf. Sci.*, 602:1299, 2008.

[65] F. C. Voogt, T. Fujii, P. J. M. Smulders, L. Nielsen, M. A. James, and T. Hibma. *Phys. Rev. B*, 60:11193, 1999.

[66] R. Pentcheva, F. Wendler, H. L. Meyerheim, W. Moritz, N. Jedrecy, and M. Scheffler. *Phys. Rev. Lett.*, 94:126101–1, 2005.

[67] H. Jahn and E. Teller. *Proc. R. Soc. London, Ser. A*, 161(905):220, 1937.

[68] D. Eisenberg and W. Kauzmann. *The Structure and Properties of Water*. Oxford University Press, New York, 1969.

[69] M. A. Henderson. *Surf. Sci. Rep.*, 46:1, 2002.

[70] P. A. Thiel and T. E. Madey. *Surf. Sci. Rep.*, 7:211, 1987.

[71] E. Ozensoy, J. Szanyi, and H. F. Peden. *J. Phys. Chem. B*, 109:3431, 2005.

[72] M. A. Henderson and S. A. Chamber. *Surf. Sci.*, 449:135, 2000.

[73] V. Maurice, S. Cadot, and P. Marcus. *Surf. Sci.*, 471:43, 2001.

[74] Y. Joseph, W. Ranke, and W. Weiss. *J. Phys. Chem. B*, 104:3224, 2000.

[75] L-Q. Wang, D. R. Baer, M. H. Engelhard, and A. N. Shultz. *Surf. Sci.*, 344: 237, 1995.

[76] M. B. Hugenschmidt, L. Gamble, and C. T. Campbell. *Surf. Sci.*, 302:329, 1994.

[77] M. Abu Haija, S. Guimond, A. Uhl, H. Kuhlenbeck, and H.-J. Freund. *Surface Science*, 600:1040, 2006.

[78] M. Kunat, S. Gil Girol, U. Burghaus, and Ch. Wöll. *J. Phys. Chem. B*, 107: 14350, 2003.

[79] C. H. Bartholomew. *Appl. Catal., A*, 212:17, 2001.

[80] D. L. Mowery, M. S. Graboski, T. R. Ohno, and R. L. McCormick. *Appl. Catal., B*, 21:157, 1999.

[81] A. V. Slack and G. A. Holliden. *Sulfur Dioxide Removal from Waste Gases, 2nd ed.* Noyes Data Corporation, Park Ridge, NJ, 1975.

[82] T. Nakatsuji and A. Miyamoto. *Catal. Today*, 10:21, 1991.

[83] A. Clark and B. Beagley. *Trans. Faraday Soc.*, 67:2216, 1971.

[84] H. Zitterer. *Gmelin Handbuch der anorganischen Chemie, S, Erg. vol 3.* Springer, Berlin, 1980.

[85] J. Haase. *J. Phys. Condens. Matter*, 9:3647, 1997.

[86] J. A. Rodriguez. *Surf. Sci.*, 226:101, 1990.

[87] S. Sakaki, H. Sato, Y. Imai, K. Morokuma, K. Ohkubo. *Inorg. Chem.*, 24: 4538, 1985.

[88] J. A. Rodriguez, P. Liu, M. Pérez, G. Liu, and J. Hrbek. *J. Phys. Chem. A*, 114:3802, 2010.

[89] J. A. Rodriguez, T. Jirsak, S. Chaturvedi, M. Kuhn, L. González, and A. Maiti. *J. Am. Chem. Soc.*, 122:12362, 2010.

[90] J. A. Rodriguez, T. Jirsak, L. González, J. Evans, M. Pérez, and A. Maiti. *Journal of Chemical Physics*, 115:10914, 2001.

[91] H. Sellers, E. Shustorovich. *Surf. Sci.*, 356:209, 1996.

[92] P. Zebisch, M. Stichler, P. Trischberger, M. Weinelt, and H.-P. Steinrück. *Surf. Sci.*, 371:235, 1997.

[93] M. Polčik, L. Wilde, J. Haase, B. Brena, G. Comelli, and G. Paolucci. *Surf. Sci.*, 381:L568, 1997.

[94] F. Hennies, A. Föhlisch, W. Wurth, P. Feulner, A. Fink, and D. Menzel. *J. Chem. Phys.*, 127:154709, 2007.

[95] D. A. Outka, R. J. Madix, G. B. Fisher, and C. DiMaggio. *J. Phys. Chem.*, 90:4051, 1986.

[96] A. R. Alemozafar and R. J. Madix. *Surf. Sci.*, 592:141, 2005.

[97] M. Polčik, L. Wilde, and J. Haase. *Phys. Rev. B*, 57:57, 1997.

[98] A. Galtayries, C. Cousi, S. Zanna, and P. Marcus. *Surf. Interface Anal.*, 36: 997, 2004.

[99] D. Stoltz, A. Önsten, U. O. Karlsson, and M. Göthelid. *Appl. Phys. Lett.*, 91:093107, 2007.

[100] J. A. Rodriguez, T. Jirsak, A. Freitag, J. Z. Larese, and A. Maiti. *Journal of Physical Chemistry B*, 104:7439, 2000.

[101] J. A. Rodriguez, G. Liu, T. Jirsak, J. Hrbek, Z. Chang, J. Dvorak, and A. Maiti. *J. of Am. Chem. Soc.*, 124:5242, 2002.

[102] J. A. Rodriguez, T. Jirsak, S. Chaturvedi, and J. Dvorak. *J. Mol. Catal. A: Chem.*, 167:47, 2001.

[103] J. A. Rodriguez, T. Jirsak, S. Chaturvedi, and M. Kuhn. *Surf. Sci.*, 442:400, 1999.

[104] S. Chaturvedi, J. A. Rodriguez, T. Jirsak, and J. Hrbek. *J. Phys. Chem. B*, 102:7033, 1998.

[105] B. J. Lindberg, K. Hamrin, G. Johansson, U. Gelius, A. Fahlman, C. Nordling, and K. Siegbahn. *Phys. Scr.*, 1:286, 1970.

[106] C. Leygraf. *Corrosion Mechanisms in Theory and Practice, Chapter 15 on Atmospheric Corrosion.* Marcel Dekker, Inc., New York-Basel, 2002.

[107] S. H. Overbury, D. R. Mullins, D. R. Huntley, and Lj. Kundakovic. *J. Phys. Chem.*, 103:11308, 1999.

[108] C. M. Pradier and P. Dubot. *J. Phys. Chem. B*, 102:5135, 1998.

[109] T. Jirsak and J. A. Rodriguez. *Langmuir*, 16:10287, 2000.

[110] G. Ruprechter and C. Weilach. *Nanotoday*, 2:20, 2007.

[111] R. T. Vang, E. Lægsgaard, and F. Besenbacher. *Phys. Chem. Chem. Phys.*, 9:3460, 2007.

[112] K. Andersson, G. Ketteler, H. Bluhm, S. Yamamoto, H. Ogasawara, L. G. M. Pettersson, and A. Nilsson. *J. Phys. Chem. C*, 111:14493, 2007.

[113] G. A. Somorjai, R. L. York, D. Butcher, and J. Y. Park. *Phys. Chem. Chem. Phys.*, 9:3500, 2007.